MEDNARODNA
PODIPLOMSKA ŠOLA
JOŽEFA STEFANA

7. ŠTUDENTSKA KONFERENCA MEDNARODNE PODIPLOMSKE ŠOLE JOŽEFA STEFANA

Zbornik - 2. del

7th JOŽEF STEFAN INTERNATIONAL POSTGRADUATE SCHOOL STUDENTS' CONFERENCE

Proceedings - Part 2

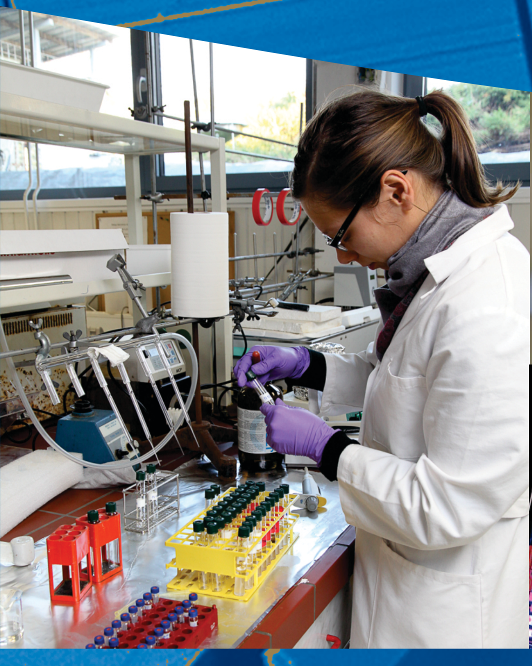

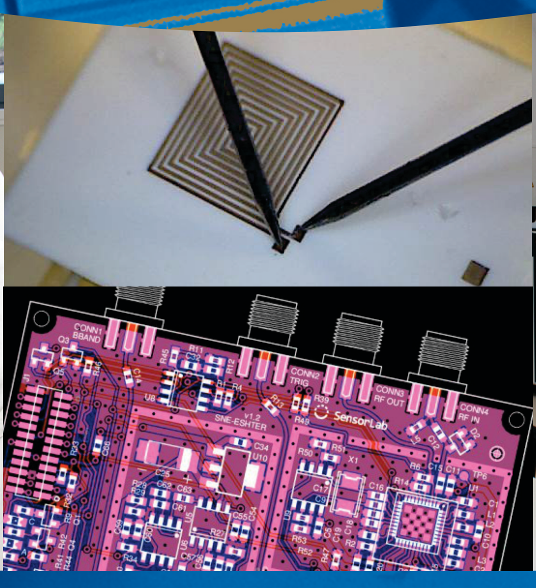

20. - 21. 05. 2015, Ljubljana

Zbornik 7. Študentske konference Mednarodne podiplomske šole Jožefa Stefana
(Proceedings of the 7th Jožef Stefan International Postgraduate School Students Conference)

Uredniki / Editors:
Andraž Rešetič
Ana Kroflič
Aleksander Matavž
Melisa Junuzović
Janja Vidmar
Maja Somrak

Založnik / Publisher:
Mednarodna podiplomska šola Jožefa Stefana, Ljubljana

Tisk / Print:
TISKARNA PLANPRINT d.o.o.

Naklada / Copies:
120 izvodov

Ljubljana, maj 2015

Konferenco organizira Študentski Svet Mednarodne podiplomske šole Jožefa Štefana
(The Conference is organized by Jožef Stefan International Postgraduate School - IPS Student Council)

CIP - Kataložni zapis o publikaciji
Narodna in univerzitetna knjižnica, Ljubljana

5/6(082)
378.046-021.68:001.891(497.4)(082)

MEDNARODNA podiplomska šola Jožefa Stefana. Študentska konferenca (7 ; 2015 ; Ljubljana)
Zbornik = Proceedings / 7. študentska konferenca Mednarodne podiplomske šole Jožefa Stefana = 7th Jožef Stefan International Postgraduate School Students' Conference, 20.-22. 5. 2015, Ljubljana ; [organizira študentski svet Mednarodne podiplomske šole Jožefa Štefana = organized by Jožef Stefan International Postgraduate School - IPS Student Council] ; uredili, edited by Andraž Rešetič ... et al.]. - Ljubljana : Mednarodna podiplomska šola Jožefa Stefana, 2015

ISBN 978-961-92871-9-4
1. Rešetič, Andraž 2. Mednarodna podiplomska šola Jožefa Stefana (Ljubljana)
279459840

7. ŠTUDENTSKA KONFERENCA MEDNARODNE PODIPLOMSKE ŠOLE JOŽEFA STEFANA

ZBORNIK - 2. DEL

7th JOŽEF STEFAN INTERNATIONAL POSTGRADUATE SCHOOL STUDENTS' CONFERENCE

PROCEEDINGS - Part 2

Uredili / Edited by

Andraž Rešetič, Ana Kroflič, Aleksander Matavž, Melisa Junuzović, Janja Vidmar
in Maja Somrak

20. - 21. 05. 2015, Ljubljana

Organizacijski odbor / Organising Committee

Redakcijski odbor / Technical Review Committee

Kazalo (Table of Contents)

Ekotehnologija (Ecotechnology) 1

Ekotehnologija (Ecotechnology)

Stability of dissolved gaseous Hg (DGM) and reactive Hg (RHg) in the absence and presence of preservatives in natural waters

Ermira Begu[1,2], Yaroslav Shlyapnikov[1,2], Kristina Obu-Vazner[2], Milena Horvat[1,2]

[1] Jožef Stefan Institute, Department of Environmental Sciences, Jamova 39, Ljubljana 1000, Slovenia

[2] Jožef Stefan International Postgraduate School, Jamova 39, Ljubljana 1000, Slovenia

ermira.begu@ijs.si

The stability of mercury species at low levels during sampling, sample handling and storage is still problematic despite all the efforts invested into this problem over the years. The problem lies in the facts that mercury species are normally present at very low concentrations in the environment, especially in natural waters, and are also unstable. The likelihood of contamination and loss of Hg during sampling, sample handling (including filtering), storage and measurement is very high. The aim of the present work is to summarize recent studies related to the stability of dissolved gaseous mercury (DGM) and reactive-Hg (RHg) in water samples. Further, we have tested the stability of DGM and RHg in fresh river waters (without addition of preservation reagent) and in distilled, fresh and marine water after acidification with HNO_3 and the addition of $AuCl_3$ as a preservative. Due to low concentrations, the samples were spiked with Hg^0 solution and Hg^{2+} standard solution. Variation of the concentrations was followed with time. DGM concentrations were determined by double amalgamation and cold vapour atomic fluorescence (CV AFS) after pre-concentration of Hg in a gold trap. RHg was determined in the same way but with the addition of tin chloride ($SnCl_2$) prior to purging. The addition of $AuCl_3$ and HNO_3 as a preservative for these Hg species, was not useful in any of the four sample matrices tested.

"Jožef Stefan" Institute, Ljubljana, Slovenia

JOŽEF STEFAN INTERNATIONAL POSTGRADUATE SCHOOL

Stability of dissolved gaseous Hg (DGM) and reactive Hg (RHg) in the absence and presence of preservatives in natural waters

Ermira Begu[1,2], Yaroslav Shlyapnikov[1,2], Kristina Obu-Vazner[2], Milena Horvat[1,2]

[1]Jožef Stefan Institute, Department of Environmental Sciences, Jamova 39, Ljubljana, Slovenia

[2] International Postgraduate School 'Jožef Stefan', Jamova 39, Ljubljana, Slovenia

Introduction

- Dissolved gaseous mercury (DGM) represent all gaseous mercury compounds in water environments (95 % of DGM is elemental mercury (Hg (0)) and <5% is dimethylmercury (DMeHg))
- The evasion of Hg (0) from oceanic waters to the global atmosphere plays an important role in the global mercury cycle
- The production of Hg(0) is a function of abiotic and biotic processes (photoreduction of Hg(II), reduction of Hg(II) by bacteria, decomposition of organic Hg, tectonic activity)
- The presence of Hg(II) (RHg) in water samples might increase the possibility of formation of MeHg (the most toxic Hg compound).
- Due to instability in long term period, the reliability of the results for DGM and RHG highly depend on the time of analysis after sampling.
- The likelihood of contamination and loss of Hg during sampling, sample handling (including filtering), storage and measurement is very high.
- We tested the storage conditions under which the losses of the Hg species of interest (DGM and RHg) in preserved and non-preserved natural water samples, are minimal.

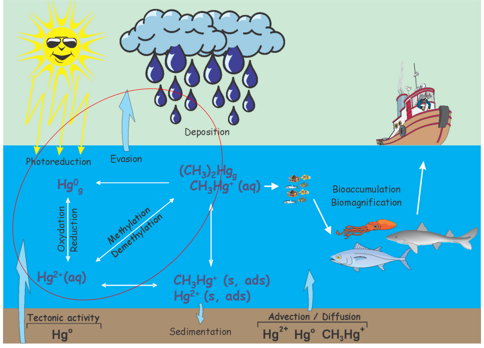

Method:

Cold vapor atomic fluorescence spectrophotometry (CV AFS) with gold pre-amalgamation.

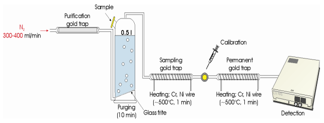

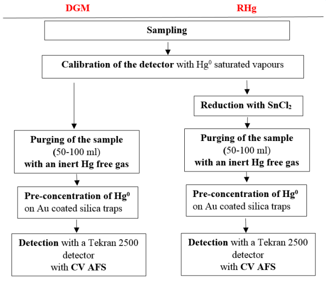

DGM	RHg
Sampling	
Calibration of the detector with Hg^0 saturated vapours	
	Reduction with $SnCl_2$
Purging of the sample (50-100 ml) **with an inert Hg free gas**	**Purging of the sample** (50-100 ml) **with an inert Hg free gas**
Pre-concentration of Hg^0 on Au coated silica traps	**Pre-concentration of Hg^0** on Au coated silica traps
Detection with a Tekran 2500 detector with **CV AFS**	**Detection** with a Tekran 2500 detector with **CV AFS**

DGM and RHg species are not stable in aqueous media for more than 5 hours, therefore timing of analysis after sampling is very important. This is a stability test for DGM and RHg in fresh waters, no preservative added.

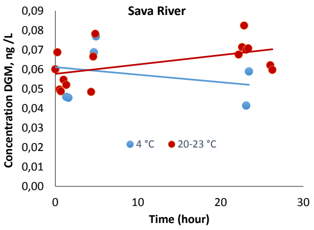

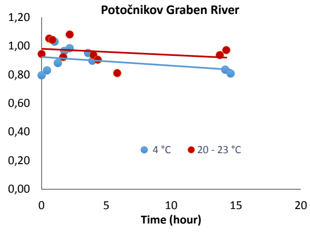

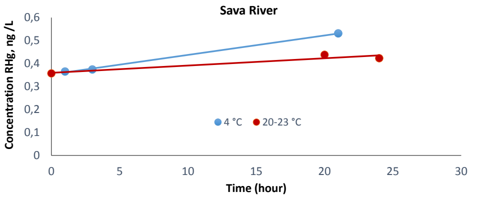

This is a stability test for DGM and RHg in waters when $AuCl_3$ and HNO_3 is added as a preservative

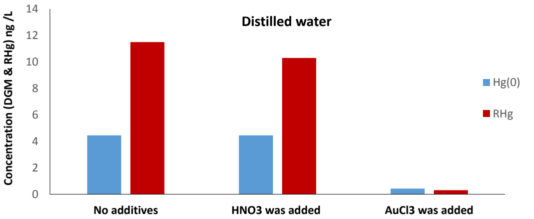

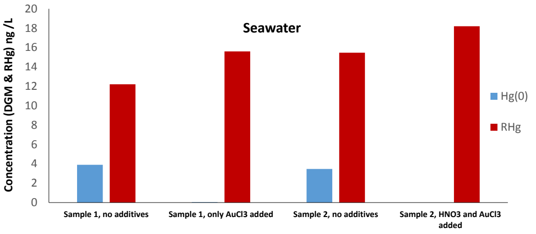

The stability of RHg in seawater after the addition of $AuCl_3xHNO_3$ (2.5 % is the difference in RHg conc. before and after the addition of the reagent)

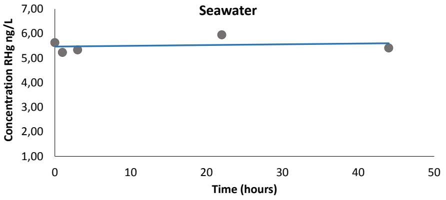

Conclusions:

1. storage of the river water at 4 ^{0}C protects concentrations of DGM over 24 hours storage period.
2. No significant changes of RHg stored at room T were observed.
3. The use of preservatives, is not proved to give good results when storing samples for DGM and RHg measurements
4. $AuCl_3$ and HNO_3, might be a good storage agent for Total Hg analysis

References:

1. Horvat M., Kotnik J., Logar M., Fajon V., Zvonarić T., Pirrone N.: Speciation of mercury in surface and deep-sea waters in the Mediterranean Sea, *Atmospheric Environment 37 Supplement No. 1 (2003) S93–S108*
2. Brown R. J. C. and Brown A. S.: Accurate calibration of mercury vapour measurements, *The Analyst (2008)*
3. US Environmental Protection Agency, Mercury Preservation Techniques

Acknowledgements:
This work is funded by the Slovenian ARRS P1-0143 programme, 7 FP GMOS and the EMRP ENV02 projects.

Assymetry of molecular processes during abscission in tomato (*Solanum lycopersicum* L.)

Marko Chersicola[1, 2], **Aleš Kladnik**[3], **Amon Lers**[4], **Marina Dermastia**[1]
[1] Department of Biotechnology and System biology, National Institute of Biology, Ljubljana, Slovenia
[2] Jožef Stefan International Postgraduate School, Ljubljana, Slovenia
[3]Department of Biology, Biotechnical Faculty, University of Ljubljana, Vecna pot 111, SI-1000 Ljubljana, Slovenia
[4]Department of Postharvest Science of Fresh Produce, ARO, The Volcani Center, Bet Dagan 50250, Israel
marko.chersicola@nib.si

Abscission is a highly regulated process in which various organs are separated from the mother plant during development. Abscission occurs specifically in the abscission zone (AZ) tissue. It has been shown that various abscission related processes occur asymmetrically between the AZ proximal and distal sides. In this study, we showed the asymmetric immunolocalization of LX ribonuclease (LX RNase) in the wild type and in LX RNase inhibited tomato lines. In addition, the expression of LX RNase gene was evaluated by real-time RT PCR both in the wild type and LX RNase inhibited lines. The findings of this study further elucidate the asymmetry of molecular processes in abscission with a potential use in biotechnology for the controlled abscission of fruits and manipulation of abscission time.

Tomato Abscission Zone

Structure and Molecular Mechanisms

Marko Chersicola[2], Aleš Kladnik[1], Marina Dermastia[2], Amnon Lers[3]

(1) Department of Biology, Biotechnical Faculty, University of Ljubljana, Vecna pot 111, SI-1000 Ljubljana, Slovenia
(2) Department of Biotechnology and Systems Biology, National Institute of Biology, Vecna pot 111, SI-1000 Ljubljana, Slovenia; marko.chersicola@nib.si
(3) Department of Postharvest Science of Fresh Produce, ARO, The Volcani Center, Bet Dagan 50250, Israel

ACC oxidase

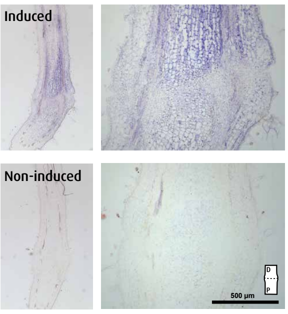

ACC oxidase immunolocalization

LX RNase

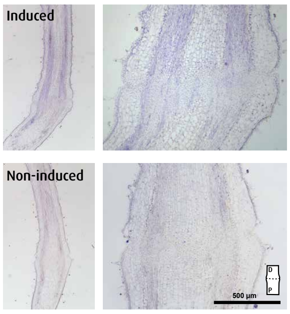

LX RNase immunolocalization

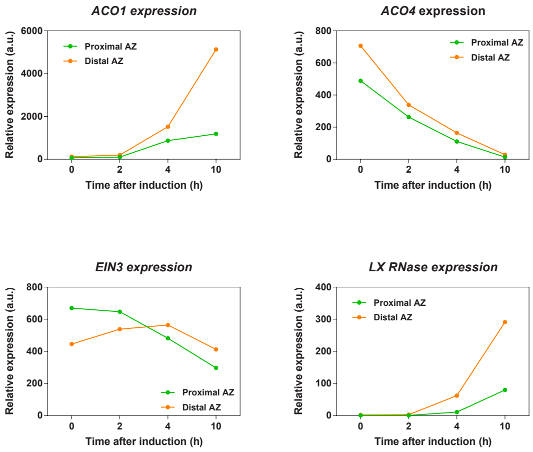

Expression analysis of selected genes in flower AZ: ACO1, ACO4, EIN3 and LX RNase relative expression measured at 0, 2, 4 and 10 hour after induction.

Sampling AZ tissue

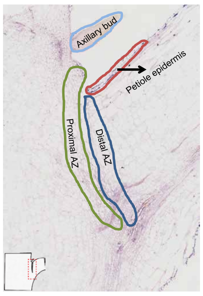

Four different zones of tissue near the fracture were sampled from sequential microscopic sections of the leaf AZ using laser microdissection and pressure catapulting (LMPC). Highlighted in green is Proximal AZ, in dark blue Distal AZ, in red Petiole epidermis and in light blue Axillary bud. From each of the zones RNA was isolated and one step RT-qPCR was performed to measure the expression of selected genes.

Flower abscission zone

Abscission zone (AZ) of the tomato flower is located in the thickened part of the flower pedicel.

Abscission is induced by cutting-off the developed flower.

AZ was separated to distal and proximal part for expression analyses.

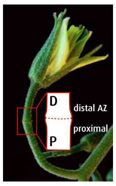

Leaf abscission zone

Abscission of the leaf petiole is induced by cutting-off the leaf blade and exposing the plant to ethylene (50 ppm).

LX RNase

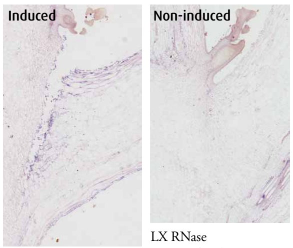

LX RNase immunolocalization

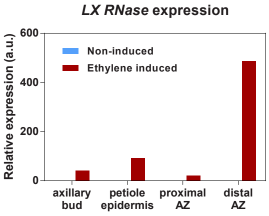

LX RNase expression measured in different parts of leaf AZ using laser capture microdissection and one step RT PCR.

ACC oxidase

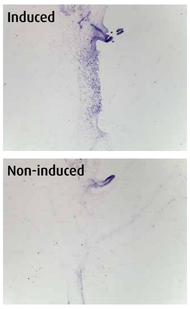

ACC oxidase immunolocalization

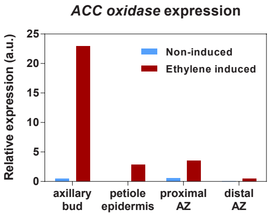

ACC oxidase expression measured in different parts of leaf AZ using laser capture microdissection and one step RT PCR.

Leaf abscission zone processes model

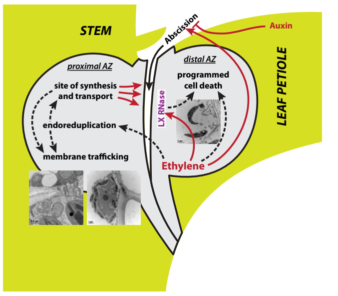

A major process on the proximal side of the AZ is endoreduplication, presumably associated with extensive membrane trafficking. Its ultrastructure is characterized by electron-lucent ameboidal-shaped nuclei, a well developed Golgi apparatus and endoplasmic reticulum connected with an elaborate plasmodesmal system, pronounced membrane invaginations, and multivesicular and paramural bodies. In addition, polygalacturonases - enzymes involved in the execution of cell separation are also located at the proximal side of the AZ. At the distal side of the AZ programmed cell death occurs. It is identified by loss of cell viability, altered nuclear morphology, DNA fragmentation, elevated levels of reactive oxygen species, and elevated enzymatic activities and expression of PCD-associated genes, including genes encoding LX ribonuclease, nuclease TBN1, cysteine and serine proteases, tomato β-1,4-endoglucanase, which is involved in cell-wall metabolism; and 1-aminocyclopropane-1-carboxylic acid synthase, involved in ethylene biosynthesis (Bar-Dror et al., 2011). Arrow-ended and blunt-ended lines represent process induction and repression, respectively, dashed lines represent putative relations.

References

1. Tal Bar-Dror, Marina Dermastia, Aleš Kladnik, Magda Tušek Žnidarič, Maruša Pompe Novak, Shimon Meir, Shaul Burd, Sonia Philosoph-Hadas, Naomi Ori, Lilian Sonego, Martin B. Dickman and Amnon Lers. ***Programmed Cell Death Occurs Asymmetrically during Abscission in Tomato***. Plant Cell 23(11): 4146-4163, November 2011.

2. Marina Dermastia, Aleš Kladnik, Tal Bar-Dror and Amnon Lers. ***Endoreduplication preferentially occurs at the proximal side of the abscission zone during abscission of tomato leaf***. Plant Signaling & Behavior 7(9), September 2012 http://www.landesbioscience.com/journals/10/article/21276/

Acknowledgement
This research was supported by research grant no. J1-5444 and P4-0165 from the Slovenian Research Agency.

NATIONAL INSTITUTE OF BIOLOGY

Iodine and selenium content in different parts of pea sprouts

Ana Jerše[1,2,] **Ana Kroflič**[1,2], **Nina Kacjan Maršič**[3], **Mateja Germ**[3], **Helena Šircelj**[3], **Radojko Jaćimović**[1], **Vekoslava Stibilj**[1,2]

[1] Department of Environmental Sciences, Jožef Stefan Institute, Ljubljana, Slovenia

[2] Jožef Stefan International Postgraduate School, Ljubljana, Slovenia

[3] Biotechincal Faculty, University of Ljubljana, Ljubljana, Slovenia

ana.jerse@ijs.si

Iodine and selenium are essential elements for humans and animals, important for normal thyroid function and thyroid hormones synthesis. Both elements come into the body by food consumption. The uptake of I and Se in pea sprouts from seeds, soaked in I and/or Se was investigated. I and Se were determined in sprouts, roots and seed residues. For iodine determination comparison between ICP-MS and k_0-INAA and for selenium determination comparison between HG-AFS and ICP-MS were done. Good agreement was observed for both comparisons. High concentrations of iodine were found in all parts of the plants, but significant difference in concentrations between different parts of the plants was observed. For selenium, high concentrations were observed, too. However, the uptake of Se(VI) was higher than the uptake of Se(IV). Iodine influenced on the selenium uptake and *vice versa*.

Iodine and selenium content in different parts of pea sprouts

Ana Jerše, Ana Kroflič, Nina Kacjan Maršič, Mateja Germ, Helena Šircelj, Radojko Jaćimović, Vekoslava Stibilj
Study programme: Ecotechnology
Supervisor: prof. dr. Vekoslava Stibilj

Jožef Stefan International Postgraduate School, Ljubljana, Slovenia
Department of Environmental Sciences, Jožef Stefan Institute, Ljubljana, Slovenia

Introduction

Iodine and selenium are essential elements for humans and animals, important for normal thyroid function and thyroid hormones synthesis. Both elements come into the body by food consumption.
Slovenia is a country with low concentrations of these elements in nutrition. For iodine, the main source is salt, but recommended decrease of salt in nutrition would reduce also the intake of iodine.
To avoid health problems caused by iodine or selenium deficiency, other food sources of these elements should be found. Naturally plants are low in concentration of both elements. However, iodine and/or selenium enriched cultivated plants could be an effective way to improve food quality and to provide sufficient intake of these elements for humans. Before the introduction of these plants into the nutrition, we have to find the appropriate way to enrich the plants with both elements.
The aim of our study was to investigate the I and Se uptake in sprouts from seeds, soaked in I and/or Se solution. Peas belong to the group of pulse and are commonly consumed vegetables that contain a high amount of albumens. The sprouts are also used in nutrition in some cultures [1–5].

Table 1: Concentrations of I and Se in some of the commonly consumed vegetables [6].

Vegetable	c(I) [ng I/g sample]	c(Se) [ng Se/g sample]
Potato	4–63	20–200
Cabbage	12–68	6–200
Soya bean	63	80–710
Bean	6–19	140–220
Pea	22–60	3–10
Pumpkin	14	-
Buckwheat	25	49

Methods

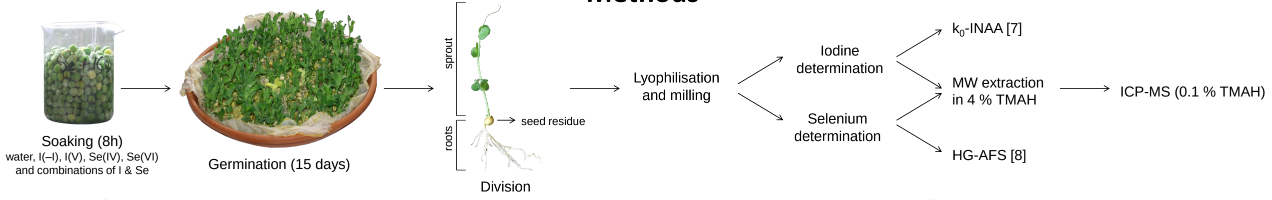

Soaking (8h)
water, I(–I), I(V), Se(IV), Se(VI) and combinations of I & Se

Germination (15 days)

sprout
roots
seed residue
Division

Lyophilisation and milling

Iodine determination
Selenium determination

k_0-INAA [7]
MW extraction in 4 % TMAH
ICP-MS (0.1 % TMAH)
HG-AFS [8]

Results and discussion

Iodine

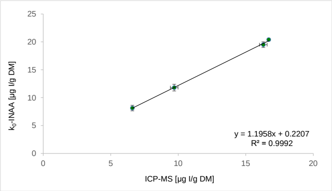

Figure 1: Comparison between I concentrations obtained by two different methods

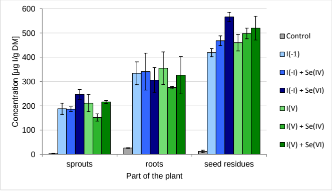

Figure 2: Iodine concentrations determined by ICP-MS in different parts of pea plants

Methods: ICP-MS and k_0-INAA as a reference method (used for some samples)
- Very good agreement
- Linear agreement also for higher concentrations (≈ 300 µg I/g DM)

Uptake
- High concentrations in all parts of the plants in comparison with control plants
- Significant difference between different parts – the lowest in sprouts, the highest in seed residues (iodine bounded on starch)
- Higher amount of I when treated with I(V) in comparison to I(–I)
- Se(IV) in sprouts– no effect on uptake of I(–I), decreased uptake of I(V)
- Se(VI) in sprouts – no effect on uptake of I(V), increased uptake of I(–I)
- Se in roots – no effect (large SD)

Selenium

Methods: HG-AFS (after acid digestion) and ICP-MS (after alkaline MW extraction)
- Good agreement

Uptake
- High amount of Se in all parts of the plants in comparison with the control plants
- In roots higher amount of Se when treated with Se(IV), in sprouts when treated with Se(VI) – easier transport of Se(VI) than Se(IV)
- I(–I) had no influence on uptake of Se (in sprouts and roots, any form of Se)
- I(V) decreased uptake of Se (in sprouts and roots, any form of Se)

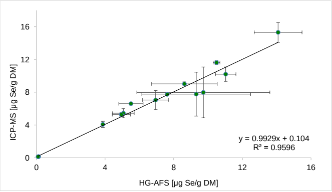

Figure 3: Comparison between Se concentrations obtained by two different methods

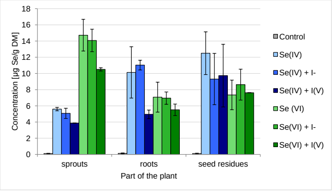

Figure 4: Selenium concentrations determined by HG-AFS in different parts of pea plants

Conclusions

- Increased concentrations of I and Se were observed in comparison with control plants.
- The lowest concentrations of iodine in sprouts, the highest in seed residues.
- Concentrations of selenium depended on its form in soaking solution.
- Se decreased or increased iodine concentrations for ± 30 %.
- I(–I) had no influence on selenium uptake.
- I(V) decreased selenium concentrations in sprouts and roots (up to – 50 %).
- The lowest concentrations of both elements obtained in plants, treated with I(V) and Se(IV) due to their higher toxicity in comparison with I(–I) and Se(VI).
- No toxicological effects on plants at selected concentrations.

References

[1] Y.G. Zhu, et al. Interactions between selenium and iodine uptake by spinach (Spinacia oleracea L.) in solution culture. *Plant and soil*, 261:99–105, 2004
[2] S. Smolen, et al. Assessment of biofortification with iodine and selenium of lettuce cultivated in the NFT hydroponic system. *Scientia Horticulturae*, 166:9–16, 2014
[3] P. Cuderman, et al. Extraction of Se species in buckwheat sprouts grown from seeds soaked in various Se solutions. *Food Chemistry*, 123:941–948, 2010*Nuclear Chemistry*, 257:259–663, 2003
[4] P. Smrkolj, et al. Respiratory potential and Se compounds in pea (Pisum sativum L.) plants grown from Se-enriched seeds. *Journal of Experimental Botany*, 57:3595–3600, 2006
[5] R. Hoover, et al. Composition, molecular structure, properties, and modification of pulse starches: a review. *Food Research International*, 45:399–413, 2010
[6] S.W. Souci, W. Fachmann and H. Kraut. *Food Composition and Nutrition Tables, 6th Edition*. H. Scherz and F. Senser, 2000.
[7] R. Jaćimović, et al. k0-INAA quality assessment by analysis of different certified reference materials using the KAYZERO/SOLCOI software. *Journal of Radioanalytical and Nuclear Chemistry*, 257:259–663, 2003
[8] P. Smrkolj, et al. Determination of selenium in vegetables by hydride generation atomic fluorescence spectrometry. *Analytica Chimica Acta*, 512:11–17, 2004

Iridium-catalysed synthesis of α-haloketones

Štefan Možina[1,2], **Antonio Bermejo Gómez**[3]**,** **Belén Martín-Matute**[3], **Stojan Stavber**[1,4], **Jernej Iskra**[4]

[1]Centre of Excellence for Integrated Approaches in Chemistry and Biology of Proteins (CIPKeBiP), Ljubljana, Slovenia

[2]Jožef Stefan International Postgraduate School, Ljubljana, Slovenia

[3]Department of Organic Chemistry and Berzelii Center EXSELENT, Arrhenius Laboratory, Stockholm University, Stockholm, Sweden

[4]Department of Physical and Organic Chemistry, Jožef Stefan Institute, Ljubljana, Slovenia

stefan.mozina@ijs.si

α-Haloketones and α-haloaldehydes are essential intermediates in organic synthesis, nevertheless their formation from unsymmetrical ketones was proven to be difficult. Selective synthesis of α-haloketones was studied by iridium catalysed 1,3-hydrogen shift of allylic alcohol with concomitant halogenation with dihaloiodonium(I) reagents. Selectivity of reaction was very sensitive on solvent mixture and by using $HIBr_2$, α-bromoketones were obtained with good conversion and high selectivity in THF/H_2O solvent mixture. On the other hand, in $EtOH/H_2O$ solvent mixture only moderate selectivity was obtained for the synthesis of α-iodoketones.

MEDNARODNA
PODIPLOMSKA ŠOLA
JOŽEFA STEFANA

JOŽEF STEFAN
INTERNATIONAL
POSTGRADUATE SCHOOL

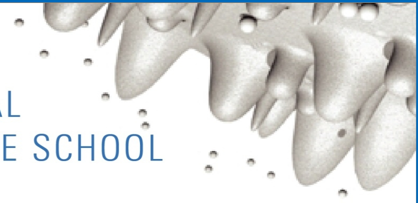

Iridium-catalysed synthesis of α-haloketones

Štefan Možina[1,2], Antonio Bermejo Gómez[3], Belén Martín-Matute[3], Stojan Stavber[1,4], Jernej Iskra[4]

[1]Centre of Excellence for Integrated Approaches in Chemistry and Biology of Proteins (CIPKeBiP), Ljubljana, Slovenia [2]Jožef Stefan International Postgraduate School, Ecotehnology, Ljubljana, Slovenia
Supervisor: izr. prof. dr. Stojan Stavber, Co-supervisor: doc. dr. Jernej Iskra

[3]Department of Organic Chemistry and Berzelii Center EXSELENT, Arrhenius Laboratory, Stockholm University, Stockholm, Sweden
[4]Department of Physical and Organic Chemistry, Jožef Stefan Institute, Ljubljana, Slovenia

Introduction

α-Haloketones are important and versatile building blocks for the synthesis of biologically active compounds. They are used for various transformations such as formation of heterocycles, C-C coupling reaction and nucleophilic substitution.[1]
Despite a number of methods have been reported for synthesis of α-haloketones and α-haloaldehydes, most have been containing only one enolizable position.[2] The same reaction on unsymmetrical ketones, which have two enolizable positions (α and α'), has been challenging and a mixture of products is usually obtained causing the challenging separation of constitutional isomers.

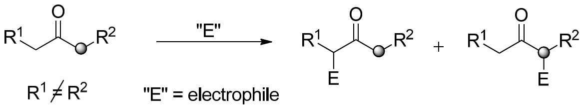

In last few years, Martín-Matute et al. reported alternative selective methods by using iridium catalyst for 1,3-hydrogen shift on allylic alcohols in presence of electrophilic halogenating reagent selective formation of α-fluoro, α-chloro and α-bromocarbonyl compounds were prepared. We envisaged that by combining iridium catalyst for 1,3-hydrogen shift on allylic alcohols and dihaloiodine(I) species we could introduce selectively iodine or bromine atom by changing reaction conditions.

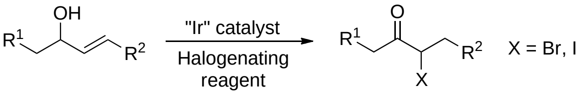

Effect of catalyst on selectivity

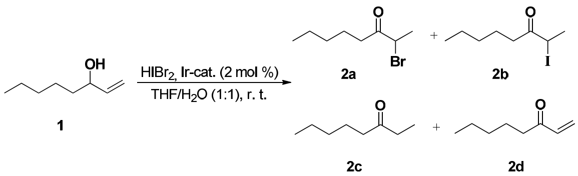

N	Catalyst	Time [h]	Conversion [%]	2a	2b	2c	2d
1	$[IrCp^*Cl_2]_2$	16	73	81	–	16	3
2	$[IrCp^*Br_2]_2$	23	77	42	–	56	2
3	**$[IrCp^*I_2]_2$**	**21**	**89**	**75**	**–**	**25**	**–**
4	$[IrCp^*(H_2O)_3]SO_4$	21	79	78	–	22	–
5	$(IrCp^*)_2(OH)_3]OH$	21	83	81	–	19	–

Effect of solvent on selectivity

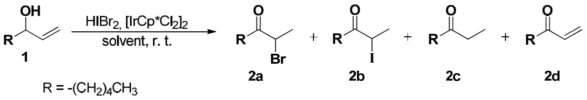

N	Solvent	Time [h]	Conversion [%]	2a	2b	2c	2d
1	$EtOH/H_2O$ (2:1)	22	60	77	–	23	–
2	$EtOH/H_2O$ (3:2)	25	58	57	12	21	2
3	$EtOH/H_2O$ (1:1)	22	70	29	31	13	7
4	**$EtOH/H_2O$ (2:3)**	**25**	**77**	**21**	**56**	**8**	**1**
5	$EtOH/H_2O$ (1:2)	22	96	10	5	9	–

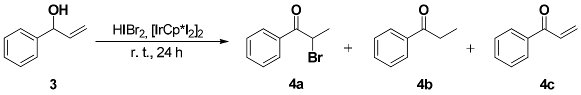

THF/H_2O (1:1); 55 % conversion; **4a/4b/4c** = 73/16/11
THF/H_2O (2:1); 78 % conversion; **4a/4b/4c** = 78/4/17

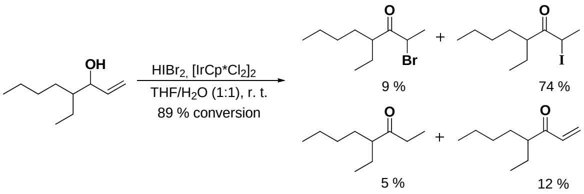

Conclusion

We have developed new efficient method for synthesis α-bromoketones and α-iodoketones which represent a large variety of building blocks. The reactions require low loading of iridium catalyst, there is no organic waste formed from halogenating reagent and it has high selectivity in case of bromination while for iodination only moderate selectivity was obtained. Further studies are being done to increase variety of allylic alcohols and with goal of improving iodination.

Reference

1. A. Erian, S. Sherif and H. Gaber, The Chemistry of α-Haloketones and Their Utility in Heterocyclic Synthesis, *Molecules*, 8, 793-865, 2003.
2. N. Ahlsten, A. Bermejo Gómez and B. Martín-Matute, Iridium-Catalyzed 1,3-Hydrogen Shift/Chlorination of Allylic Alcohols, *Angewandte Chemie International Edition*, 52, 6273-6276, 2013.

cipkebip
Centre of excellence for integrated approaches in chemistry and biology of proteins
cost
EUROPEAN COOPERATION IN SCIENCE AND TECHNOLOGY
Institut
"Jožef Stefan"
Ljubljana, Slovenija

Determination of geographical origin of milk in Slovenian by elemental and stable isotope analysis

Igor Perišić[1,2] , Doris Potočnik[1,2], Marijan Nečemer[3], Darja Mazej[1], Nives Ogrinc[1,2]
[1] Department of Environmental Sciences, Jožef Stefan Institute, Ljubljana, Slovenia
[2] Jožef Stefan International Postgraduate School, Ljubljana, Slovenia
[3] Department Low and Intermediate Energy Physics
igor.perisic@ijs.si

The presented work uses stable isotope ratios and elemental composition to determine the regional provenance of milk. The first database of authentic Slovenian cow milk has been established. The database includes isotope values of oxygen and hydrogen ($\delta^{18}O$ and $\delta^{2}H$) in milk, the isotopic composition of carbon and nitrogen in casein ($\delta^{13}C$ and $\delta^{15}N$) and the elemental composition from four different geographical regions in Slovenia: the Alps, the Dinaric Alps, the Pannonian Plain and the Mediterranean.

Stable isotope data were obtained by measurements on Isotope Ratio Mass Spectrometry (IRMS). Concentrations of P, S, Cl, K, Ca, Zn, Br, Rb, Sr were analysed using reflection X-ray fluorescence spectrometry (XRF), while trace elements (Mn, Fe, Cu, As, Se, Cd, Pb) were determined using inductively coupled plasma mass spectrometry (ICP-MS). The results show that the use of stable isotopes in a combination with elemental composition is the most appropriate method for verifying the declared geographical origin. The most significant variables were Cl, Ca, Zn, K in $\delta^{13}C$ during summer, while in winter Cl, K, P, S, Mn and $\delta^{15}N$ were more significant. The overall prediction ability was 91.4%. This research represents a part of the ERA Chair ISO-FOOD for isotope techniques in food quality, safety and traceability.

Institut
"Jožef Stefan"
Ljubljana, Slovenija

ISO Fd Food ERA Chair
Safety
Quality
Traceability

MEDNARODNA PODIPLOMSKA ŠOLA JOŽEFA STEFANA
JOŽEF STEFAN INTERNATIONAL POSTGRADUATE SCHOOL

Determination of geographical origin of milk in Slovenia by elemental and stable isotope analysis

Igor Perišić[1,2] , Doris Potočnik[1,2], Marijan Nečemer[3], Darja Mazej[1], Nives Ogrinc[1,2]

[1] Department of Environmental Sciences, Jožef Stefan Institute, Ljubljana, Slovenia
[2] Jožef Stefan International Postgraduate School, Ljubljana, Slovenia
[3]Department Low and Intermediate Energy Physics

Milk contains numerous nutrients and it makes a significant contribution to meeting the body's need for calcium, magnesium, selenium, riboflavin, vitamin B12 and pantothenic acid (vitamin B5). The quality of food products as well as the quality of milk is closely linked to its geographical origin. The determination of the geographic origin of milk and milk products has recently become possible, by measuring the stable isotopes ratios of oxygen ($\delta^{18}O$) in milk water together with the hydrogen (δ^2H), nitrogen ($\delta^{15}N$), and carbon ($\delta^{13}C$) isotope contents of specific milk fractions. The presented work uses stable isotope ratios and elemental composition from four different geographical regions in Slovenia: the Alps, the Dinaric Alps, the Pannonian Plain and the Mediterranean.

Sampling

- Performed two times per year (June and December).
- Different geographical regions in Slovenia (Alpine, Mediterranean, Dinaric and Pannonian).
- Samples stored at -20^{0}C before analysis.

Analytical method

- δ^2H and $\delta^{18}O$ directly in milk after equilibration with CO_2 by using IRMS (GV instruments) with IsoPrime MultiFlow Bio equilibration unit.
- $\delta^{13}C$ and $\delta^{15}N$ in casein - Europa Scientific 20-20 with ANCA-SL .
- Concentration of macro- and micro- elements (P, S, Cl, K, Ca, Zn, Br, Rb, Sr, Fe): total X-ray Fluorescence Spectrometry (TXRF).
- Trace elements (Cu, Pb, Se, As, Cd, Ni, Mn): ICP-MS.
- Statistical evaluation: Liner Discriminant Analysis (LDA).

Tab1e 1: The summary of stable isotope and elemental data in Slovenian milk in December 2013.

Parameters	*Mediterranean*	*Pannonia*	*Alpine*	*Dinaric*
Stable isotopes				
$\delta^{18}O_{water}$ (‰)	-5.0 ± 0.5	-5.3 ± 0.4	-5.2 ± 0.8	-5.3 ± 0.6
$\delta^{13}C_{casein}$ (‰)	-24.9 ± 2.3	-21.0 ± 1.1	-23.0 ± 1.6	-22.3 ± 2.1
$\delta^{15}N_{casein}$ (‰)	4.2 ± 0.7	6.5 ± 0.5	5.7 ± 1.1	5.8 ± 0.6
Macro and micro elements				
Ca (mg/ 100 g)	110 ± 14	113 ± 11	113 ± 15	111 ± 14
K (mg/100 g)	128 ± 20	145 ± 14	146 ± 20	144 ± 18
Cl (mg/ 100 g)	74 ± 17	84 ± 9	89 ± 10	91 ± 13
S (mg/100 g)	24 ± 3	27 ± 4	26 ± 5	28 ± 5
P (mg/ 100 g)	62 ± 12	77 ± 10	78 ± 13	76 ± 12
Na (mg/ 100 g)	33 ± 4	35 ± 2	35 ± 3	33 ± 7
Zn (µg/100 g)	329 ± 57	392 ± 28	374 ± 34	368 ± 34
Br (µg/ 100 g)	147 ± 32	106 ± 14	139 ± 40	197 ± 71
Rb (µg/100 g)	190 ± 100	196 ± 67	210 ± 63	215 ± 40
Sr (µg/ 100 g	27 ± 6	29 ± 5	30 ± 15	20 ± 7
Fe (µg/ 100 g)	33 ± 3	25 ± 6	28 ± 5	29 ± 5
Trace elements				
Ni (µg/ 100 g)	4.5 ± 0.7	4.6 ± 1.2	4.5 ± 1.0	5.6 ± 1.1
Mo (µg/ 100 g)	7.4 ± 1.2	7.5 ± 2.5	8.7 ± 1.8	8.8 ± 2.2
Mn (µg/ 100 g)	3.9 ± 0.9	2.8 ± 1.1	2.4 ± 0.8	2.9 ± 0.8
Cu (µg/ 100 g)	7.0 ± 3.4	4.6 ± 1.2	4.4 ± 1.4	5.3 ± 1.5
Se (µg/ 100 g)	2.0 ± 0.2	1.6 ± 0.4	1.6 ± 0.5	2.0 ± 0.8
As (µg/ 100 g)	0,043 ± 0.004	0.042 ± 0.017	0.043 ± 0.015	0.057 ± 23
Cd (µg/ 100 g)	0.006 ± 0.004	0.005 ± 0.003	0.004 ± 0.002	0.007 ± 0.004
Pb (µg/ 100 g)	0.076 ± 0.051	0.055 ± 0.035	0.0076 ± 0.057	0.064 ± 0.027

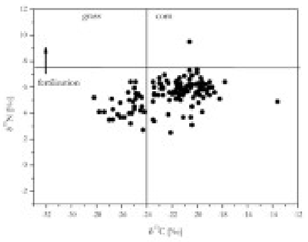

Figure 1: The relationship between $\delta^{13}C$ and $\delta^{15}N$ in milk casein.

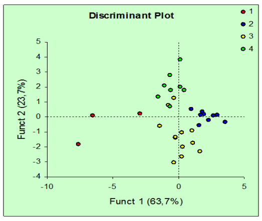

Figure 2: Discrimination between geographical regions was performed with LDA using significant isotopic and elemental parameters. Function 1 represents 63.7% of variability, while function 2 represents 23.7% of variability. Macro-regions: 1 - Mediterranean, 2 – Pannonia, 3 – Alpine, 4 – Dinaric.

Results

- The mean difference between milk and cow drinking water was 11% for δ^2H values (1σ = 3%) and 2.2% for $\delta^{18}O$ values (1σ = 0.7%). Seasonal differences are quite obvious. The differences obtained in δ^2H and $\delta^{18}O$ in milk from different geographical areas can be explained by environmental and ecophysiological factors that affect the isotopic composition of water and the resulting milk.

- $\delta^{13}C$ values vary between -28.5 and -18.7 ‰, while $\delta^{15}N$ values vary between 4.2 and 8.6 ‰ in casein of cow's milk between different geographic areas. The combination of $\delta^{13}C$ and $\delta^{15}N$ values provide useful information about the geographical and agricultural origin of milk and thus on its quality.

Conclusion

Stable isotope ratios and major/trace elements are complementary and very useful for the determination of origin. Most of these parameters are however influenced by the season due to variation in the forage composition. It was found that stable isotope data and elemental composition can differentiate between the milk from different geographical regions in Slovenia.

ACKNOWLEDGEMENTS:
The work was performed within the project **V4-1108** entitled "The use of specific methods for determination and prevention of adulteration of milk and dairy products" financially supported by Slovenian Research Agency and Ministry of Agriculture and the Environment. We thank Ljubljanske mlekarne, d.d., Pomurske mlekarne, d.d., Mlekarna Vipava d.d., Mlekarna Planika predelava mleka d.o.o. and Mlekarna Celeia for supplying cow samples.
The research is also supported by the felowship of Ad Futura and represent a part of the Era Chair ISO-FOOD project.

Characterization of Slovenian milk using the composition and stable isotopes of fatty acids

Doris Potočnik[1,2], **Nives Ogrinc**[1,2]
[1] Department of Environmental Science, Jožef Stefan Institute, Ljubljana, Slovenia
[2] Jožef Stefan International Postgraduate School, Ljubljana, Slovenia
Doris.potocnik@ijs.si

Milk and dairy products are important everyday nutrition and are a major source of fat and fatty acids in the human diet. Because of their importance, they are in considerable demand and are relatively expensive. Since it is possible, in dairy industry, to influent the quality of milk products, the determination of geographical origin represents an important strategic issue for providers and consumers. In this study fatty acid (FA) composition is used to obtain information about authenticity of milk. Milk samples from different geographical regions in Slovenia (Alpine, Pannonia, Dinaric, Mediterranean) were collected two times per year and used to determine the content, as well as isotopic composition, of individual FA. FA composition was determined using the *in-situ trans*-esterification method and characterized by gas chromatography with FID detector (GC-FID), while compound specific isotope ratio mass spectrometry (CS-IRMS) was used to determine the isotopic composition of individual FA.

ISO-FOOD received funding from the European Union's Seventh Framework Programme for research, technological development and demonstration under grant agreement no 621329 (2014-2019).

Characterization of Slovenian milk using stable isotope composition and fatty acids

Doris Potočnik[1,2], Nives Ogrinc[1,2]
[1] Department of Environmental Science, Jožef Stefan Institute, Ljubljana, Slovenia
[2] Jožef Stefan International Postgraduate School, Ljubljana, Slovenia

The development and application of analytical tools for the verification of geographical origin, production origin and species origin of food products is one of the main topics in food science, since it is possible, in dairy industry, to influence the quality of milk products. Thus the determination of geographical origin represents an important strategic issue for providers and consumers. The presented work uses stable isotope ratios and fatty acids to determine the regional provenance of milk. The first database of authentic Slovenian cow milk has been established. The database includes isotope values $\delta^{13}C$ of individual fatty acid and the fatty acids composition in milk from four different geographical regions in Slovenia: the Alps, the Dinaric region, the Pannonia region and the Mediterranean.

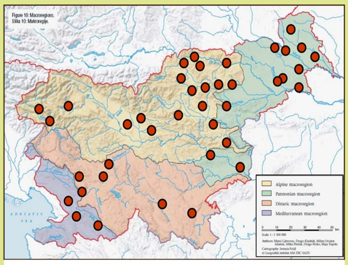

Figure 1: Sampling location

SAMPLING:

40 samples of authentic cow milk, 2 time per year (summer, winter), from different geographical regions (Mediterranean, Pannonia, Dinaric and Alpine) in Slovenia

ANALYTHICAL METHOD:

- determination of fatty acids composition in milk using gas chromatography (GC-FID)
- determination of $\delta^{13}C$ in FA using and GC-C-IRMS

GC-C-IRMS

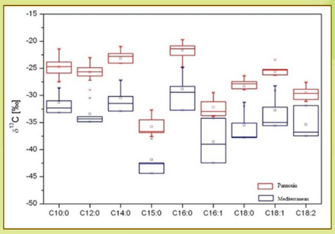

Figure 2: Stable carbon isotope composition for individual fatty acids for Mediterranean and Pannonia region. $\delta^{13}C$ values in FAs from Mediterranean were lower comparing to $\delta^{13}C$ values of Pannonia region, which indicated than corn was more often nutrient use for cow in Pannonia region.

GEOGRAPHICAL ORIGIN:

The isotopic composition of dairy products reflects the dietary regime and the metabolism of the milk producing animals.

- The climatic condition such as temperature and humidity are known to promote shift in $\delta^{13}C$ isotopic values in plants from different regions due to effects of evapotranspiration and photosynthesis.

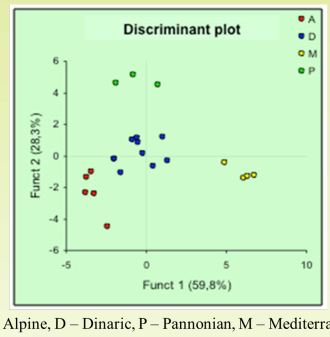

A – Alpine, D – Dinaric, P – Pannonian, M – Mediterranean

Figure 3: Classification of milk samples according to the geographical origin in relation to the content of fatty acids. Milk samples from different geographical areas are statistically separated. The main parameters that contributed to the separation were conjugated linoleic acid (CLA), C14:0, C16:0.

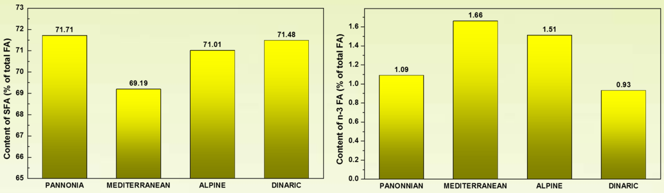

Figure 4: Content of saturated fatty acids and ω-3 fatty acids in milk. In milk fat, where dairy cows are associate with grazing, high concentration of ω-3 (especially C18:3ω–3) and lower concentration of SFA may be observed.

The work was performed within the project V4-1108 entitled “The use of specific methods for determination and prevention of adulteration of milk and dairy products” financially supported by Slovenian Research Agency and Ministry of Agriculture and the Environment. We thank Ljubljanske mlekarne, d.d., Pomurske mlekarne, d.d., Mlekarna Vipava d.d., Mlekarna Planika predelava mleka d.o.o. and Mlekarna Celeia for supplying cow samples.

www.isofood.eu

Sizing of nanoscale titanium dioxide and its quantification in the presence of dissolved titanium by single particle inductively coupled plasma mass spectrometry

Janja Vidmar[1,2], **Radmila Milačič**[1,2], **Janez Ščančar**[1,2]

[1] Department of Environmental Sciences, Jožef Stefan Institute, Ljubljana, Slovenia
[2] Jožef Stefan International Postgraduate School, Ljubljana, Slovenia
janja.vidmar@ijs.si

As a consequence of their applications in various industrial products, titanium dioxide nanoparticles (TiO_2NPs) have been released into the environment where they can act as stressors towards biota. In the present work, a new analytical approach was applied for the determination of total concentration and size distribution of TiO_2NPs in anatase and rutile in aqueous samples by the use of single particle inductively coupled plasma mass spectrometry (SP-ICP-MS). It requires minimal sample preparation, offers superior sensitivity, and enables simultaneous characterization of analyte in nanosize and dissolved form. For SP-ICP-MS measurements, suspensions of NPs must be sufficiently diluted (ng L^{-1} level) and short integration time (10 ms or less) used in order to measure the intensity of single particle as a single pulse. Under such conditions, the frequency of pulses is proportional to the number concentration of NPs and the number of counts of each pulse is related to the NP size. The accuracy of the quantification of TiO_2NPs by SP-ICP-MS was verified by calculating the recoveries between the determined and expected Ti concentrations, while calculated size distributions were checked by comparison with manufacturer reported sizes. To the best of our knowledge, this study is the first report on simultaneous quantitative determination of nanosize Ti and its dissolved forms by SP-ICP-MS. The procedure developed can be applied to the analysis of different TiO_2NPs in environmental water samples.

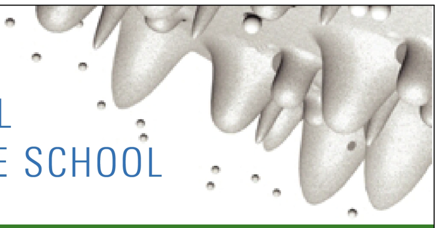

Sizing of nanoscale titanium dioxide and its quantification in the presence of dissolved titanium by SP-ICP-MS

Janja Vidmar, Radmila Milačič, Janez Ščančar
Department of Environmental Sciences, Jožef Stefan Institute, Ljubljana, Slovenia
Jožef Stefan International Postgraduate School (Ecotechnology), Ljubljana, Slovenia

1. INTRODUCTION

As a consequence of their extensive use in various applications, titanium dioxide nanoparticles (TiO_2NPs) have been released into environment, where act as stressors towards biota. In this study, new analytical approach was applied for the determination of the total concentration and size distribution of TiO_2NPs in anatase and rutile in aqueous samples by the use of single particle ICP-MS.

2. METHODS

Sample preparation

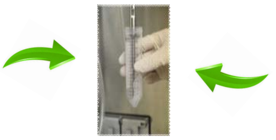

rutile
(<100 nm)

anatase
(<25 nm)

ultrasonic homogeniser, applied for 3 min

SP-ICP-MS operating parameter (7700x Agilent)	
Nebuliser	MicroMist
Nebulizer pump	0.3 rps
Collision gas flow rate (He)	4.3 mL min^{-1}
Data acquisition mode	TRA
Integration time per isotope	10 ms
Total acquisition time	100 s
Isotopes monitored	^{48}Ti

3. RESULTS

Determination of TiO_2NPs size distribution

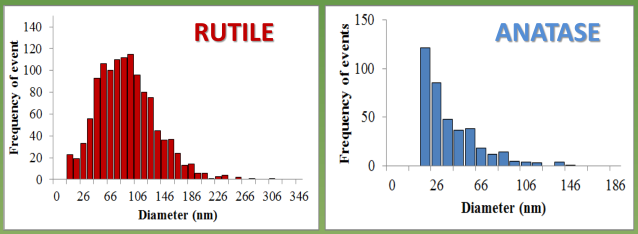

Mean diameter, determined by SP-ICP-MS, for TiO_2NPs in anatase is 32 nm and for TiO_2NPs in rutile is 107 nm.

Simultaneous quantification of dissolved Ti and TiO_2NPs

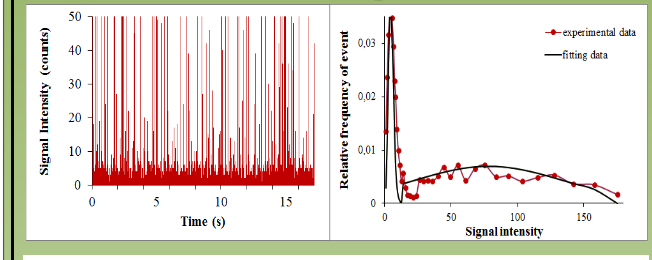

Time scan and signal distribution histogram for the mixture of TiO_2NPs (rutile) and dissolved Ti.

	Ti(IV) added ng mL^{-1}	TiNP added ng mL^{-1}	Ti(IV) measured ng mL^{-1}	TiNP measured ng mL^{-1}	Recovery TiNP (%)
RUTILE	0.500	0.298	0.456 ± 0.031	0.298 ± 0.034	100
	0.05	0.032	0.047 ± 0.003	0.031 ± 0.002	97
ANATASE	0.500	0.580	0.525 ± 0.024	0.480 ± 0.020	83
	0.05	0.0348	0.063 ± 0.001	0.030 ± 0.003	87
	0.05	0.0580	0.056 ± 0.001	0.056 ± 0.001	97

Recoveries between the determined and expected Ti mass concentrations in TiO_2NPs in the presence of dissolved Ti by the use of SP-ICP-MS.
Overlapping between dissolved and particulate signal distribution increases with decreasing NPs size, causing lower recoveries for TiO_2NPs in anatase.

4. CONCLUSIONS

SP-ICP-MS enables quantitative determination of the mass concentration and size distribution of TiO_2NPs in aqueous suspensions of anatase and rutile. The accuracy of the determination of Ti mass concentration in TiO_2NPs was verified by the calculation of the recoveries between the determined and added Ti. The determined size distribution agreed with manufacturer reported sizes. In addition, SP-ICP-MS technique enabled also simultaneous quantification and sizing of TiO_2NPs and its dissolved forms. The procedure developed extends the applicability of SP-ICP-MS for sizing and quantification of TiO_2NPs in environmental water samples.

Conceptual model of Ljubljansko polje aquifer

Janja Vrzel[1,2], Goran Vižintin[3], Nives Ogrinc[2,4]

[1] Ecological engineering institute d.o.o., Maribor, Slovenia

[2] Jožef Stefan International Postgraduate School, Ljubljana, Slovenia

[3] Department of Mining and Geotechnology, Faculty of Natural Sciences and Engineering, Ljubljana, Slovenia

[4] Department of Environmental Sciences, Jožef Stefan Institute, Ljubljana, Slovenia

janja.vrzel@ijs.si

The regional steady state model of groundwater flow in Ljubljansko polje aquifer is under preparation. It will provide a framework for the development of regional transient state groundwater flow model, which will be extended into transport model, where $\delta^{18}O$, $\delta^{2}H$ and ^{3}H isotopes will be used as transport materials. The model is constructed with software FEFLOW® 6.1. At the present the conceptual model with precise geometry of the study area is available. The model will extend our knowledge about interactions between surface and groundwater.

CONCEPTUAL MODEL OF LJUBLJANSKO POLJE AQUIFER

Janja Vrzel[a,d], Goran Vižintin[b], Nives Ogrinc[c,d]

[a]*Ecological engineering institute d.o.o., Maribor, Slovenia*
[b]*Depratment of Mining and Geotechnology, Faculty of Natural Sciences and Engineering, Ljubljana, Slovenia*
[c]*Department of Environmental Sciences, Jožef Stefan Institute, Ljubljana, Slovenia*
[d]*International Postgraduate School Jožef Stefan, Ljubljana, Slovenia*

Investing in your future
OPERATION PART FINANCED BY THE EUROPEAN UNION
European Social Fund

Numerical models help us to understand the complex nature of groundwater systems. Their start is somewhat parallel with development and widespread availability of faster workstations. Many codes were written to solve the governing equations for the different spatial, geological and hydrological conditions, since than.

The aim of our work is to develop a regional steady state model that will provide a framework for the development of regional transient groundwater model for the whole Ljubljansko polje aquifer system. The groundwater will be extended into a transport model, which will be used for interpretation of $\delta^{18}O$, $\delta^{2}H$ and ^{3}H isotopes in the aquifer. The model is constructed with the finite element flow simulation system FEFLOW® 6.1 from MIKE Powered by DHI.

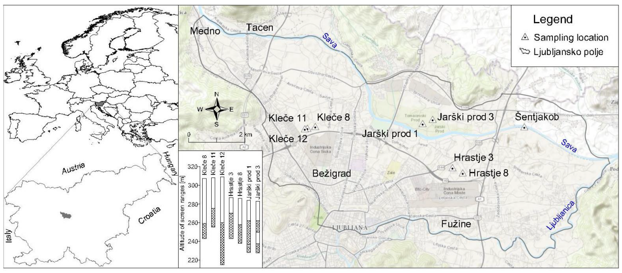

Figure 1: Study area with sampling locations.

CONCEPTUAL MODEL

Figure 2: Outcrops of hardpan in Tacen.

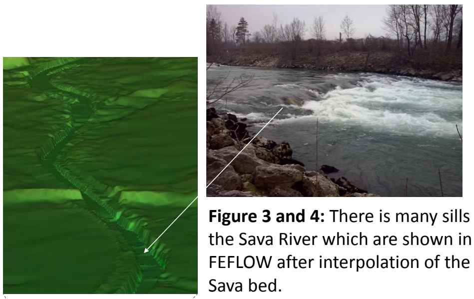

Figure 3 and 4: There is many sills in the Sava River which are shown in FEFLOW after interpolation of the Sava bed.

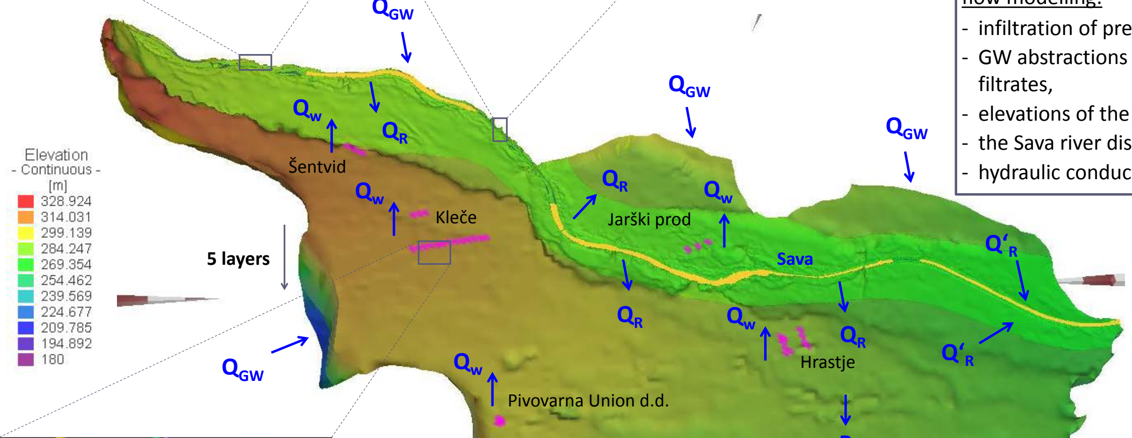

Q_{GW}

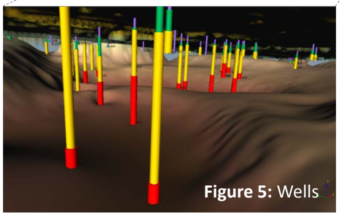

Figure 5: Wells

Data required for the geometry construction:

- 115 drilling reports & geological studies of Ljubljansko polje,
- the counter hard pen map (Permian and Carboniferous rocks).
- River cross-sections
- LiDAR data
- DMR

Data required for groundwater (GW) flow modelling:

- infiltration of precipitation,
- GW abstractions and depths of the filtrates,
- elevations of the GW table,
- the Sava river discharges,
- hydraulic conductivities.

Legend:

Q_{GW} – Underground inflow
Q_{R} – Infiltration of the Sava river
Q'_{R} – GW infiltration into the Sava
Q_{W} – groundwater abstraction in Kleče, Jarški prod, Hrastje, Šentvid and Pivovarna Union d.d.
P_{I} – Infiltration of precipitation

ACKNOWLEDGMENT

The model is under preparation as a part of the on going EU 7th Research Project – GLOBAQUA (Managing the effects of multiple stressors on aquatic ecosystem under water scarcity). The research is partially supported by the Environmental Social Found (KROP 2012). The authors would like to thank all those who allow to use their data: Javno Podjetje Vodovod-Kanalizacija Ljubljana, The City Municipality of Ljubljana, Holding Slovenske Elektrarne d.o.o., Pivovarna Union d.d., Slovenian Environmental Agency and The Surveying and Mapping Authority of the Republic of Slovenia.

Jožef Stefan Institute Ljubljana, Slovenija

Investing in your future
Operation part financed by the European Union
European Social Fund

GOZDARSKI INŠTITUT SLOVENIJE
SLOVENIAN FORESTRY INSTITUTE

KARST RESEARCH INSTITUTE POSTOJNA

MEDNARODNA PODIPLOMSKA ŠOLA JOŽEFA STEFANA
JOŽEF STEFAN INTERNATIONAL POSTGRADUATE SCHOOL

Can soil CO_2 fluxes be affected by subterranean cave systems?

Bor Krajnc[1], Mitja Ferlan[2], Nives Ogrinc[3]

[1] Jožef Stefan International Postgraduate School, Ljubljana, Slovenia, bor.krajnc@ijs.si;
[2] Department of Forest Ecology, Slovenian Forestry Institute, Ljubljana, Slovenia, mitja.ferlan@gozdis.si;
[3] Department of Environmental Sciences, Jožef Stefan Institute, Ljubljana, Slovenia, nives.ogrinc@ijs.si

1 INTRODUCTION: Main factors affecting soil CO_2 fluxes in most terrestrial ecosystems are soil temperature and soil moisture. Nevertheless occasionally high soil CO_2 fluxes were observed at karst areas, which could result from ventilation of subterranean cavities [1]. Accurate estimations of ecosystem CO_2 fluxes are important for determination and quantification of the system CO_2 sinks or sources. CO_2 concentrations and ^{222}Rn activity concentrations were measured in cave air as indirect indicators of cave ventilation, while stable isotope composition of CO_2 was used to determine its possible sources.

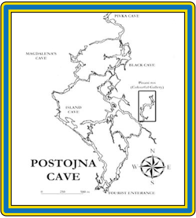

Figure 1: Location of Pisani rov in Postojna Cave (adopted from [4])

Figure 2: Scheme of underground chamber system

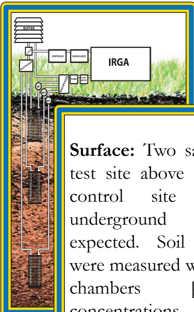

2 STUDY AREA: Pisani rov (Colourful Gallery), a dead-end passage is a 920 m long horizontal passage which deviates from the main Postojna Cave passage to the north (Fig. 1) and terminates below the the Velika Jeršanova doline where the thickness of the cave celling is estimated to be around 30 m [2]. Cave air sampling location is at the end of Pisani rov. Soil air sampling locations are in the forest above the cave. (Fig. 7).

3 METHODS:
Cave: Sampling performed twice a month from October 2013. Stable isotope composition of cave air CO_2 was determined with CF-IRMS (EUROPA 20-20) connected to ANCA-TG preparation module. CO_2 concentration was measured with TESTO 435, multi-functional measurement instrument. ^{222}Rn activity concentrations were determined with alpha-scintillation cells.

Surface: Two sampling sites: test site above the cave and control site where no underground cavity is expected. Soil CO_2 fluxes were measured with automatic chambers [3]. CO_2 concentrations, temperatures and carbon stable isotope composition of soil air at three different depths (0.2 m, 0.5 m and 0.8 m) were determined using subsurface chambers (Fig.2). Soil CO_2 concentration was measured using an Infra-Red Gas Analyser (IRGA) (Li-840 Li-cor, Inc., Lincoln, Nebraska

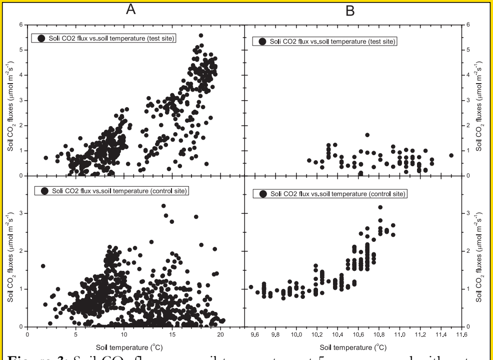

Figure 3: Soil CO_2 fluxes vs. soil temperature at 5 cm measured with automatic chambers (A) and subsurface chambers preliminary measurements (B)

4 RESULTS and DISCUSSION:

Cave ventilation: During the warm season CO_2 in the cave accumulates and during the cold season the cave ventilates (Fig.4). When the soil is covered with snow and outside temperatures are below freezing point, CO_2 starts to accumulate again. ^{222}Rn concentrations and pCO_2 are well correlated showing a common driving force.

Soil CO_2 fluxes: Results from the preliminary test (Fig.3(B)), showsw CO_2 fluxes at the control plot in a good correlation with soil temperatures ($r = 0.79$, $p = 0.01$). Soil CO_2 fluxes at the test plot did not show statistically significant correlations with soil temperatures or soil moisture. However, latter measurements form automatic chambers show different behaviour ($r = 0.70$, $p = 0.05$) and no correlation at control plot. These results do not necessarily deny the hypothesis that cave ventilation influences soil CO_2 flux at that site, but can be also consequence of extremely humid and rainy year and the difference between soil types between sites.

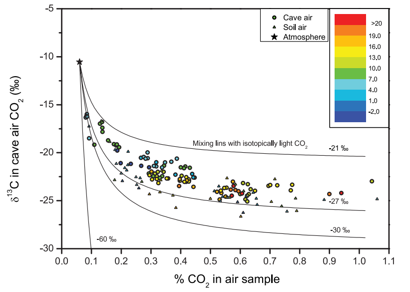

Figure 6: Plot of soil and cave air CO_2 concentrations vs. its ^{13}C isotope composition. Data is colour maped according to outside temperature during sampling. Lines represent two endmember mixing between atmosphere air and isotopically light CO_2.

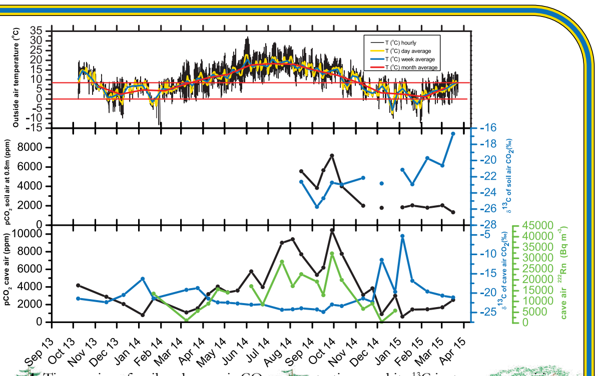

Figure 4: Time series of soil and cave air CO_2 concentrations and its ^{13}C isotope composition, ^{222}Rn concentration in cave air and Postojna air temperatures with marked lines of cave temperature of 8.4 °C and 0°C

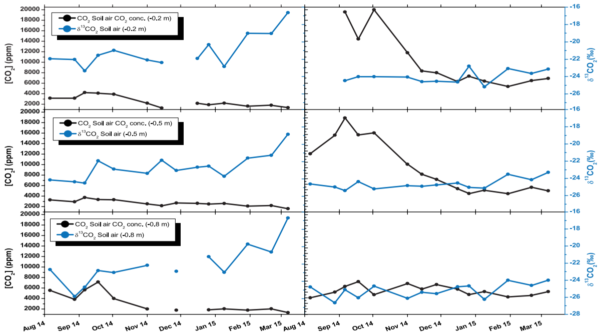

Figure 5: Time series of soil CO_2 concentrations and its ^{13}C isotope compositions on test and control sites, at three different depths (0.2, 0.5 and 0.8 m)

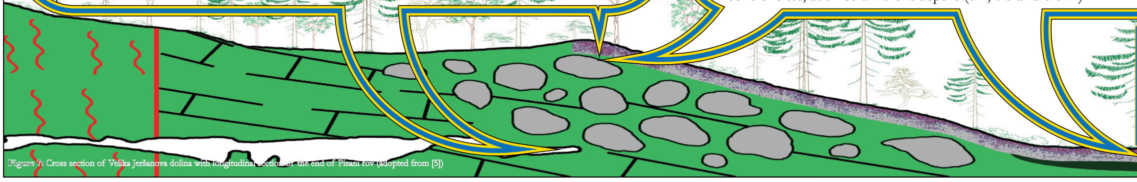

Figure 7: Cross section of Velika Jeršanova dolina with longitudinal section of the end of Pisani rov (adopted from [5])

6 REFERENCES

[1] M. Ferlan, G. Alberti, K. Eler, F. Batič, A. Peressotti, F. Miglietta, A. Zaldei, P. Simončič, D. Vodnik. Comparing carbon fluxes between different stages of secondary succession of a karst grassland. *Agriculture, Ecosystems & Environment*, 140 (1-2): 199–207, 2011.

[2] S. Šebela. Accesses from the surface to the Postojna Cave system. *Annales. Series historia naturalis*, 20 (1): 55–64, 2010.

[3] Ferlan, Mitja., Batic, Franc., Simoncic, Primoz (2013): The use of micro-meteorological methods for the monitoring of the carbon fluxes in Karst ecosystems. Doctoral dissertation = Spremljanje toka ogljika v kraskih ekosistemih z mikrometeoroloskimi metodami : doktorska disertacija. [M. Ferlan], Ljubljana.

[4] T.R. Shaw. *Names from the past in Postojnska jama (Postojna cave)*. ZRC Publishing, 2006.

[5] S. Šebela and J. Čar. Velika Jeršanova doline - a former collapse doline = Velika Jeršanova dolina - nekdanja udornica. *Acta carsologica*, 29 (2): 201–212, 2000.

Informacijske in komunikacijske tehnologije (Information and Communication Technologies)

Developing API for efficient and secure access to IoT resources and data

Matej Celarc[1]**, Adnan Bekan**[1, 2]**, Matevž Vučnik**[1, 2]**, Mihael Mohorčič**[1, 2]
[1] Department of Communication Systems, Jožef Stefan Institute, Ljubljana, Slovenia
[2] Jožef Stefan International Postgraduate School, Ljubljana, Slovenia
matejcelarc@gmail.com

In this paper we present a solution for an IoT platform API, based on an example IoT platform Videk. The platform runs several services with different requirements, such as database manipulation using CRUD operations, future-proof architecture with machine and human readable resource representation, real-time data delivery and security. We developed an API using REST architecture style and WebSocket protocol for real-time data delivery. Performance evaluation of the proposed API confirmed its suitability also for collecting measurements in fast changing environment and dynamically configurable connected devices.

MEDNARODNA
PODIPLOMSKA ŠOLA
JOŽEFA STEFANA

JOŽEF STEFAN
INTERNATIONAL
POSTGRADUATE SCHOOL

Developing API for efficient and secure access to IoT resources and data

Matej Celarc[1], Adnan Bekan[1,2], Matevž Vučnik[1,2], Mihael Mohorčič[1,2]
[1] Department of Communication Systems, Jožef Stefan Institute, Ljubljana, Slovenia
[2] Jožef Stefan International Postgraduate School, Ljubljana, Slovenia

REQUIREMENTS

- **Storing measurement** data to the platform database
- Retirieving **historical data** from the database with **query parameters**
- Retrieving historical data and **real-time data**
- Device management
- Scalable architecture
- URI scheme based on database resources
- Security

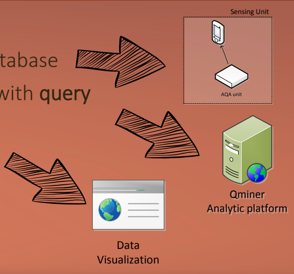

API is a set of instructions, an interface for software-to-software communication, which allows a platform to access data from its database, sensor nodes and/or other services.

SOLUTION

Videk platform architecture with the proposed example API

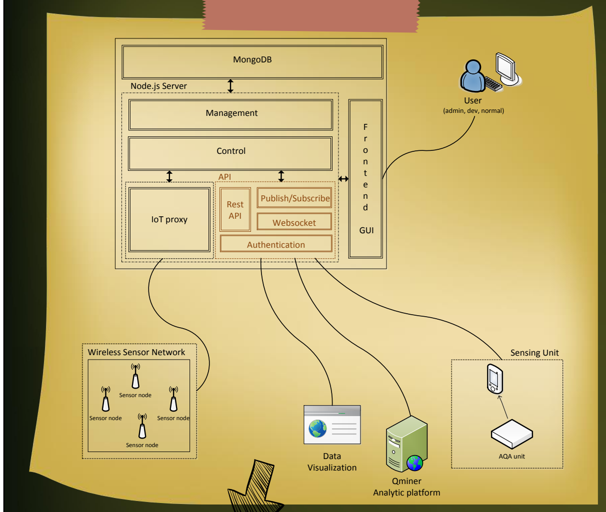

EVALUATION

- HTTP long-polling vs WebSocket
- elapsed time between measurement insertion and web browser reception
- mean average sum of elapsed times for different number (n) of inserted measurements, test was repeated 10 times

n	long-polling	WebSocket	ratio
1	75,4	6,7	11,253731
10	221,8	23,6	9,3983051
100	1288,4	179,7	7,1697273
500	4769,3	915,8	5,2077965
1000	8738,6	1442,3	6,058795
5000	55134,8	7427,9	7,4226632
10000	139603,2	14467,8	9,6492349

RESTful API

- HTTP protocol
- stateless, authorization header is needed with every request
- resources ace accessed over HTTP methods POST, GET, PUT, DELETE
- Query parameters
- resource URIs:

URI	Available methods
/api	GET
/api/nodes	GET, POST
/api/nodes/:node_id	GET, PUT, DELETE
/api/clusters	GET, POST
/api/clusters/:cluster_id	GET, PUT, DELETE
/api/sensors	GET, POST
/api/sensors/:sensors_id	GET, PUT, DELETE
/api/measurements	GET, POST
/api/measurements/:measurements_id	GET, PUT, DELETE

WEBSOCKET API

- bidirectional communication over single TCP connection
- reduced network traffic and latency (fast)
- publish/subscribe mechanism
- senders subscribe messages to channels, receivers subscribe to these channel
- channels = measurements from specific sensor

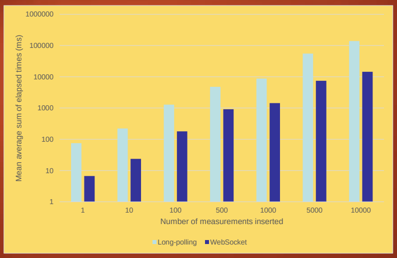

CONCLUSION

In order to provide a fast API for real-time updates, it makes sense to take advantage of the benefits that the WebSocket protocol brings. WebSocket protocol is faster than HTTP long-polling by a factor of 5 to 11!

sensorlab.ijs.si

Condition monitoring of mechanical drives based on entropy indices

Boštjan Dolenc [1,2], **Pavle Boškoski** [1], **Đani Juričić** [1]

[1] Department of Systems and Control, Jožef Stefan Institute, Ljubljana, Slovenia

[2] Jožef Stefan International Postgraduate School, Ljubljana, Slovenia

bostjan.dolenc@ijs.si

Reliable fault diagnosis of mechanical drives can become nontrivial task in case of restricted instrumentation and variable operating conditions. Under such circumstances changes in the calculated features cannot be unambiguously associated with change in system condition. In this paper we propose a feature appropriate for diagnosing faults in mechanical drives that is robust to fluctuations in operating conditions. Moreover, its time evolution seems to be correlated only with the machine condition. Instead of relying on spectral properties of the vibrational signal, we rather observe changes in the statistical patterns of the derived distribution functions. The effectiveness of the algorithm was evaluated on three datasets comprising both gear and bearing faults under constant and variable load. Additionally, the newly proposed feature was adapted for condition monitoring of the turbine of milling machine. The proposed methodology shows considerable correlation between feature and the actual state of milling machine.

Boštjan Dolenc (bostjan.dolenc@ijs.si)
Mentor: prof. dr. Đani Juričić
Dept. of Systems and Control

Condition monitoring of mechanical drives based on entropy indices

Condition-based maintenance recommends maintenance actions based on the information collected through on-line condition monitoring. In order to optimise maintenance strategy, a time-to-failure or at least the condition of the machine needs to be known prior to its final failure. With such information at hand, maintenance action can be done at optimal time and the machines life can be fully exploited.

Problem statement

Reliable fault diagnosis of mechanical drives can become nontrivial task in case of restricted instrumentation and variable operating conditions. Under such circumstances changes in the classical features [1] cannot be unambiguously associated with change in system condition. A robust condition monitoring feature can be built by characterising the distribution of energy in the generated vibrations [2].

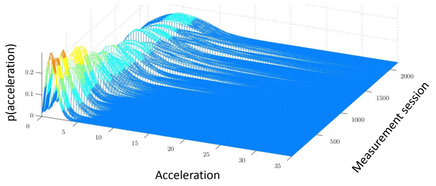

Figure 1: Envelope pdfs of the generated vibrations of gear experiment under variable load: narrow pdfs belong to the fault-free operation.

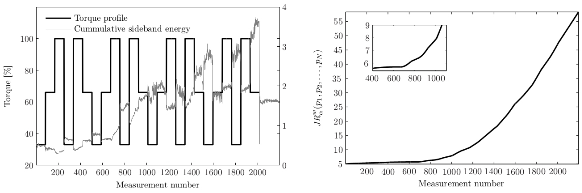

Figure 2: Classical features (left) vs. JR features (right) for the gear experiment under variable load: The influence of load variations is clearly visible in classical features. Without precise load measurements it is impossible to determine the proper cause for the abrupt changes in the features, while JR divergence remains unaffected.

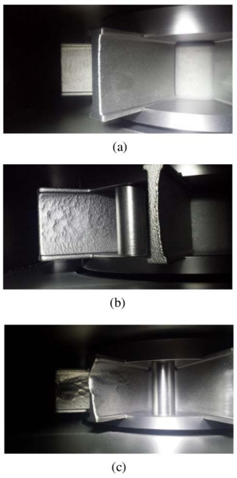

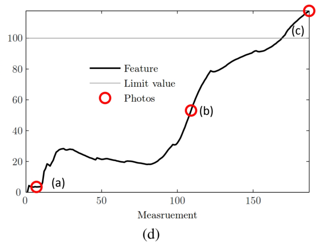

Figure 3: The correlation between fault progression and evolution of the entropy health index for the milling machine. Figures (a-c) correspond to the time points indicated by red circles on the health index plot (d).

The main idea

By monitoring statistical properties of the generated vibrations detect change in machine‘s condition.

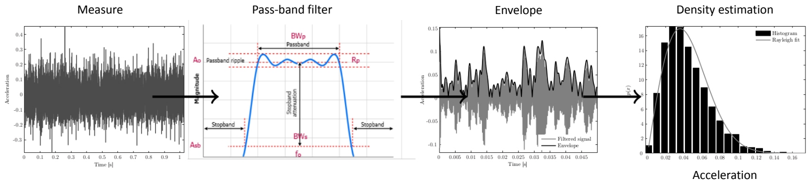

Apply generalised Jensen-Renyi (JR) divergence to quantify the change in envelope probability density function (pdf) *after each measurement session*:

$$JR^w_\alpha(\mathcal{P}_1,\dots,\mathcal{P}_n) = R_\alpha\left(\sum_{i=1}^{n} w_i\mathcal{P}_i\right) - \sum_{i=1}^{n} w_i R_\alpha\left(\mathcal{P}_i\right),$$

$$\text{where } w_i = C\cdot e^{-\frac{\lambda}{n}i} \text{ and } \sum w_i \equiv 1$$

where P_i denote envelope pdfs obtained from measured vibrations, w_i are weighting coefficients and R_α is Renyi entropy.

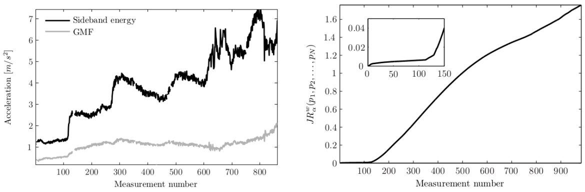

Figure 4: The evolution of two classical spectral features from the gear experiment under constant load (left): amplitude of the spectral component at the gear mesh frequency (GMF) and sideband energy. Even under constant operating conditions classical features show non-monotonic behaviour while JR divergence (right) increases with growing surface defect.

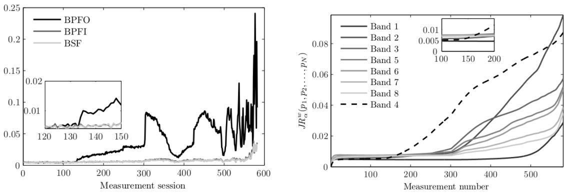

Figure 5: Results from bearing experiment. At the beginning, the JR divergence (right) is almost zero. As surface faults start to emerge, around the 130th measurement session, the JR divergence starts to increase. Unlike the standard features (left), the increase of the JR divergence is monotone. Note that divergence was evaluated in 8 frequency bands, hence 8 values. Band No. 4 corresponds to the band where classical features were calculated.

Works Cited

[1] A. K. S. Jardine, D. Lin and D. Banjevic, “A review on machinery diagnostics and prognostics implementing condition-based maintenance,” *Mechanical Systems and Signal Processing*, vol. 20, pp. 1483-1510, 2006.

[2] P. Boškoski and Đ. Juričić, “Fault detection of mechanical drives under variable operating conditions based on wavelet packet Rényi entropy signatures,” *Mechanical Systems and Signal Processing*, vol. 31, pp. 369-381, 2012.

And others cited in the paper.

Towards Unobtrusive Stress Detection

Martin Gjoreski[1,2], **Hristijan Gjoreski**[1,2], **Mitja Lušterk**[1,2], **Matjaž Gams**[1,2]

[1] Department of Intelligent Systems, Jožef Stefan Institute, Ljubljana, Slovenia
[2] Jožef Stefan International Postgraduate School, Ljubljana, Slovenia
martin.gjoreski@ijs.si

This paper presents a machine-learning method for unobtrusive stress detection system. The idea is to automatically monitor three components of the stress response, i.e. emotional, behavioural and physiological. The emotional response is monitored using smartphone's microphone and emotional voice analysis. The physiological response is monitored using a sensor-equipped wristband and bio-signal analysis. And, the behavioural response is monitored using smartphone's sensors and smartphone-usage analysis. All three modules are combined using machine-learning methods to predict stress levels. We present approaches to monitor three components of the stress response with preliminary results and an indication of the feasibility of the proposed system.

Department of Intelligent Systems
Jožef Stefan Institute
Ljubljana, Slovenia

TOWARDS UNOBTRUSIVE STRESS DETECTION

MARTIN GJORESKI, Hristijan Gjoreski, Mitja Luštrek, Matjaž Gams
Information and Communication Technologies,
Jožef Stefan International Postgraduate School
Jožef Stefan Institute

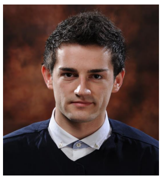

Motivation

- Among the negative consequences of chronic stress are raised blood pressure, bad sleep, increased vulnerability to infections, slower body recovery processes, and overall decreased mental performance.
- The National Alliance on Mental Illness's survey revealed that **64%** of the students who drop out of college do so for mental health reasons.
- The cost to **Europe** of work-related mental health problems in 2013 was estimated to **€617 billion** annually.
- In **Slovenia**, the economic costs for work-related stress in 2009 was estimated to **€1.2 billion**, or approximately €1.300 per worker annually.
- A system for early **detection of stress** leading to appropriate counter-measures could improve many aspects of human life, including general health, education and economy.

Proposed approach for stress detection

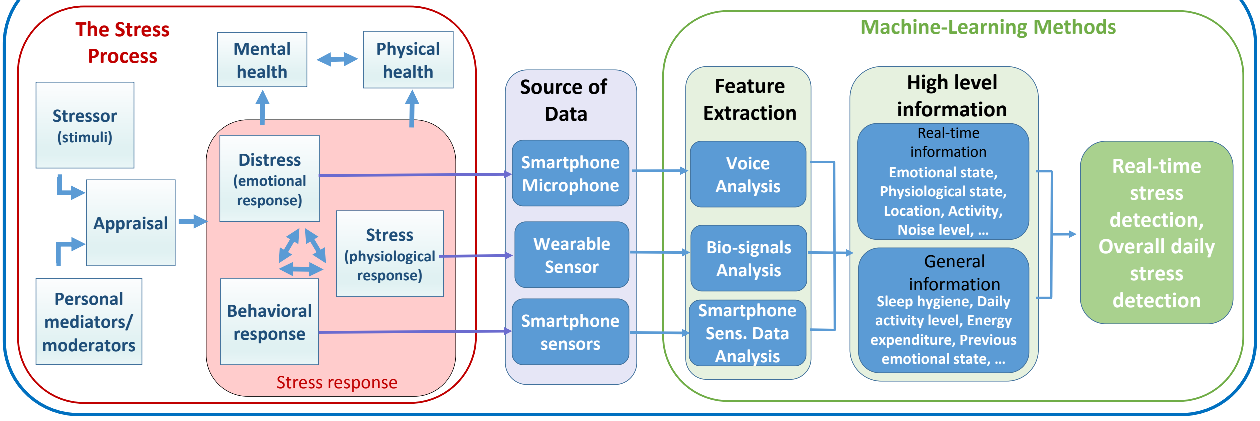

The Stress Process

Stressor (stimuli)

Appraisal

Personal mediators/ moderators

Mental health

Physical health

Distress (emotional response)

Stress (physiological response)

Behavioral response

Stress response

Source of Data

Smartphone Microphone

Wearable Sensor

Smartphone sensors

Machine-Learning Methods

Feature Extraction

Voice Analysis

Bio-signals Analysis

Smartphone Sens. Data Analysis

High level information

Real-time information
Emotional state, Physiological state, Location, Activity, Noise level, …

General information
Sleep hygiene, Daily activity level, Energy expenditure, Previous emotional state, …

Real-time stress detection, Overall daily stress detection

Stress - Emotional response

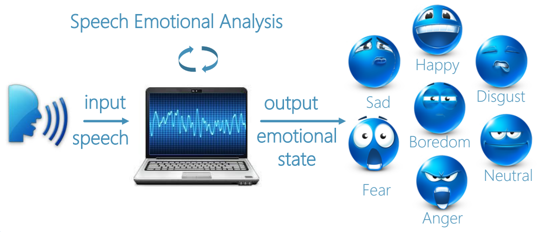

Speech Emotional Analysis

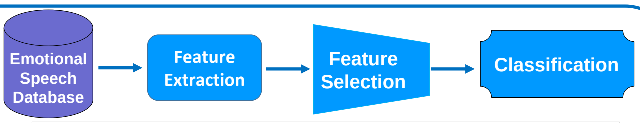

Emotional Speech Database → Feature Extraction → Feature Selection → Classification

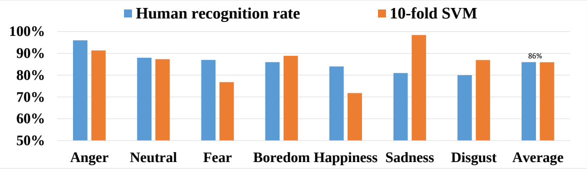

Stress - Behavioral response

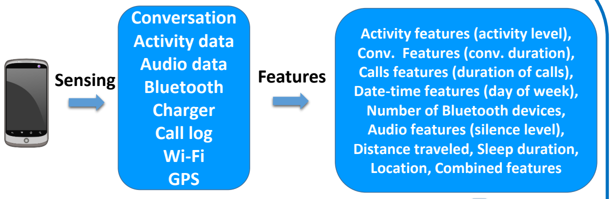

Sensing

Conversation
Activity data
Audio data
Bluetooth
Charger
Call log
Wi-Fi
GPS

Features

Activity features (activity level), Conv. Features (conv. duration), Calls features (duration of calls), Date-time features (day of week), Number of Bluetooth devices, Audio features (silence level), Distance traveled, Sleep duration, Location, Combined features

ML

User-Specific Machine-Learning Model

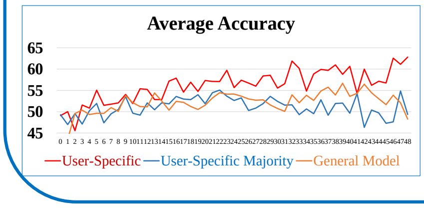

Stress - Physiological response

An example for physiological signs (sweating rate and heart rate) for real-life stressful event. The subject is taking a group exam (several students at once). The exam lasted three hours including two presentations and one question-answering session per student.

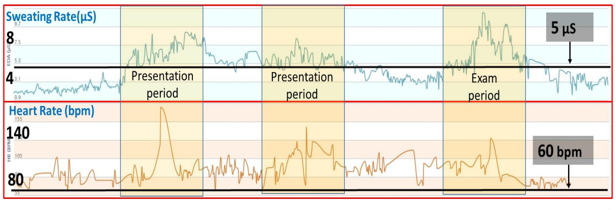

Improving QSAR models by exploiting unlabeled data from public databases of bioactive drug-like molecules

Jurica Levatić[1,2], **Fran Supek**[3,4], **Sašo Džeroski**[1,2]

[1] Department of Knowledge Technologies, Jožef Stefan Institute, Ljubljana, Slovenia

[2] Jožef Stefan International Postgraduate School, Ljubljana, Slovenia

[3] Division of Electronics, Institut Ruđer Bošković, Zagreb, Croatia.

[4] Centre for Genomic Regulation and Universitat Pompeu Fabra, Barcelona, Spain

jurica.levatic@ijs.si

Quantitative structure-activity relationship (QSAR) modelling is concerned with predicting biological effects of chemicals, with the aim of reducing the cost and duration of drug development. Due to the expensive annotation procedure, labeled datasets are often small in the domain of QSAR modelling, but unlabeled data are abundant. This represents a limitation for traditional supervised machine learning methods, which rely on labeled data only. On the contrary, semi-supervised methods use both labeled and unlabeled data, with the goal to improve performance of supervised methods. In this work, we explore the possibility of exploiting public databases of drug-like molecules as a source of unlabeled data for semi-supervised learning. To develop QSAR models, we use our recently proposed semi-supervised method based on predictive clustering trees for multi-target regression. The results show that unlabeled molecules extracted from the ChEMBL database helped to improve the predictive performance of the QSAR model for predicting cytostatic properties of potential antimalarial medications on human cells. This suggests that public databases can indeed be used as a valuable source of unlabeled data to improve performance of QSAR models – at no additional cost.

MEDNARODNA
PODIPLOMSKA ŠOLA
JOŽEFA STEFANA

JOŽEF STEFAN
INTERNATIONAL
POSTGRADUATE SCHOOL

Improving QSAR models by exploiting unlabeled data from public databases of bioactive drug-like molecules

Jurica Levatić[1,2], **Fran Supek**[3,4], **Sašo Džeroski**[1,2]
Supervisor: Prof. Dr. Sašo Džeroski, Study programme: Information and Communication Technologies
[1] Department of Knowledge Technologies, Jožef Stefan Institute, Ljubljana, Slovenia
[2] Jožef Stefan International Postgraduate School, Ljubljana, Slovenia
[3] Division of Electronics, Institut Ruđer Bošković, Zagreb, Croatia.
[4] Centre for Genomic Regulation and Universitat Pompeu Fabra, Barcelona, Spain

Motivation

- Pharmaceutical industry spends huge amounts of money on research and development of new drugs: **$1.3 billion** and **12 years of R&D** to bring a new drug to market
- Only a small fraction of promising drugs will ever progress to clinical trials due to the undesired chemical properties
- Quantitative structure-activity relationship (QSAR) models can considerably reduce this cost by predicting chemical properties of a molecule without the need to synthesize it
- The number of labeled data used to train QSAR models is typically very small, presenting a limiting factor for machine learning methods
- Semi-supervised machine learning methods can overcome this limit by using unlabeled data, in addition to labeled

Novel semi-supervised method for multi target regression

- Multi-target regression (MTR) is a structured output prediction task where the goal is to simultaneously predict multiple continuous target variables
- Semi-supervised methods able to solve MTR problems are scarce
- We propose semi-supervised method based on self-training of ensembles of predictive clustering trees (PCTs) for MTR

Self-training for MTR

Input: - learning method f (Random forest of PCTs for MTR)
- labeled data L, unlabeled data U

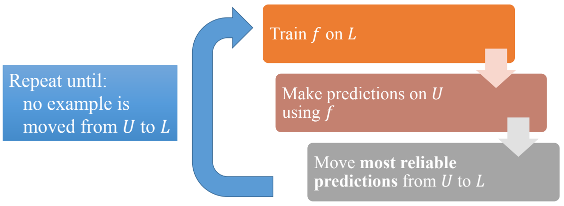

Repeat until:
no example is moved from U to L

Train f on L

Make predictions on U using f

Move **most reliable predictions** from U to L

- Self-training strongly relies on the assumption that its own (most reliable) predictions are correct
- The most crucial part of the algorithm is to define a proper reliability scoring function
- We use the variance of the votes of an ensemble as an indicator of reliability

Idea: Prediction is reliable if the predictions of the individual trees in the random forest are coherent

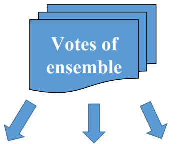

Votes of ensemble

	Target 1	Target 2	Target 3
Vote 1	0.5	6.7	3.2
Vote 2	1.23	6.72	2.23
Vote 3	0.22	5.9	1.8
Vote 4	0.78	4.5	3.4
…	…	…	…
StdDev	0.43	0.24	0.76

Application: antimalarial drugs

- We build QSAR model for prediction of 12 different properties of primaqune-like molecules:
  - cytostatic activity against 8 different human tumor cell lines
  - free radical scavenging ability (interaction with DPPH)
  - inhibition of the soybean lipoxygenase enzyme
  - inhibition of lipid peroxidation
- Labeled dataset consists of 40 primaquine-like molecules which are under consideration as novel antimalarial medications
- We extract unlabeled data for semi-supervised learning from the ChEMBL database – public database containing ~1.5 million of bioactive drug-like small molecules

Results

- Our semi-supervised method (CLUS-SSL) outperformed supervised random forest (CLUS-RF) on 10 out of 12 target variables

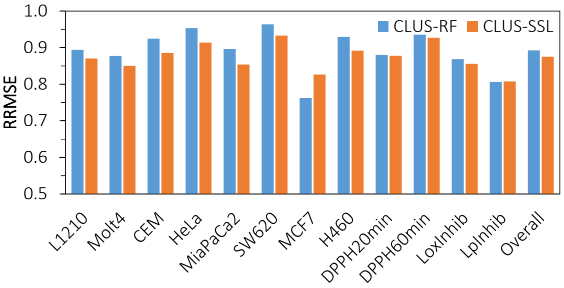

Conclusions

- The results show that accuracy of the QSAR model is improved by the use of unlabeled data extracted from the ChEBML database
- This suggest that public databases of compounds can be used to improve traditional QSAR models - at no additional cost

Nanoznanosti in nanotehnologije (Nanosciences and Nanotechnologies)

Comprehensive transformation of alcohols catalysed by new type of metal-free and acid-free catalysts under solvent-free reaction conditions

Njomza Ajvazi[1] and Stojan Stavber[2,3]
[1] Jožef Stefan International Postgraduate School, Ljubljana, Slovenia
[2] Department of Organic and Bioorganic Chemistry, Jožef Stefan Institute, Ljubljana, Slovenia
[3] Centre of excellence for integrated approaches in chemistry and biology of proteins
`njomzaajvazi@hotmail.com`

We introduce a new type of metal-free and acid-free catalysts for comprehensive transformation of various types of alcohols with different nucleophile sources under high substrate concentration reaction conditions (HCRC) or solvent-free reaction conditions (SFRC). In the absence of nucleophile, dimerization occurred, in the presence of methanol, etherification took place, while in the case of electro-rich alkenes, aryls or β-dicarbonyl compounds, new C-C bond were formed, and in the presence of acetonitrile or anilines, C-N bond were formed. When trimethyl substituted silanes were used, as sources of nucleophiles, halogenation, etherification or isothiocyanation took place, while in some cases silylation was observed.

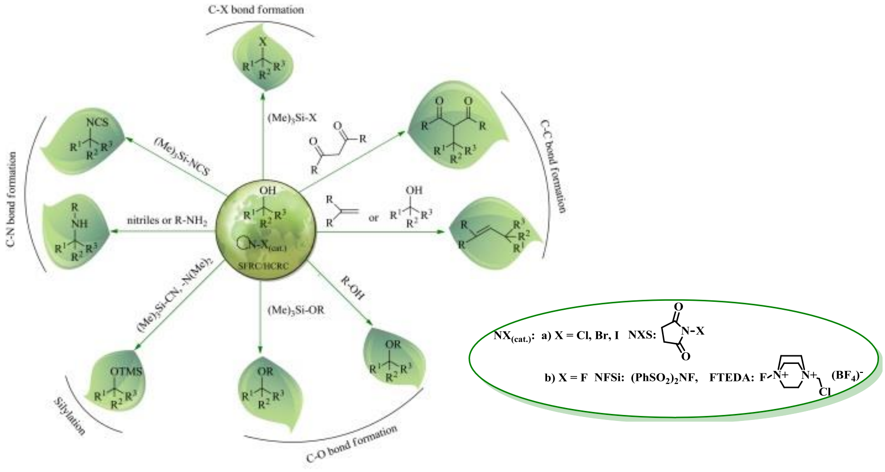

MEDNARODNA
PODIPLOMSKA ŠOLA
JOŽEFA STEFANA

JOŽEF STEFAN
INTERNATIONAL
POSTGRADUATE SCHOOL

Comprehensive transformation of alcohols catalysed by new type of metal-free and acid-free catalysts under solvent-free reaction conditions

Njomza Ajvazi[1] and Stojan Stavber[2,3]

Study program: Nanosciences and Nanotechnology
[1] Jožef Stefan International Postgraduate School, Ljubljana, Slovenia
[2] Jožef Stefan Intstitute, Ljubljana, Slovenia
[3] Centre of excellence for integrated approaches in chemistry and biology of proteins, Ljubljana, Slovenia

INTRODUCTION

Since alcohols are versatile compounds, their direct transformation under green reaction conditions would be important process to provide useful building blocks in organic synthesis Numerous related methodologies have been elaborated using catalytic amount of molecular iodine[1], metals such as indium[2] or iridium[3] and Bronsted acids such as *p*-toluensulfonic acid[4] or trifluoromethanesulfonic acid[5].

Aim of this work: New methodology for comprehensive direct transformation of various alcohols catalysed by new type of metal-free and acid-free, environmentally acceptable, selective and efficient catalysts in order to obtain new **C-C** and **C-heteroatom** bond formation under **solvent-free reaction conditions (SFRC)** or **high substrate concentration reaction conditions (HCRC).**

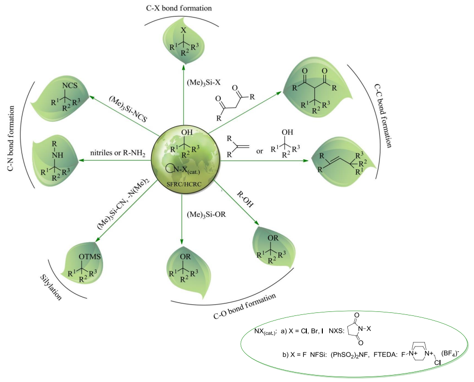

General concept and work-plan of the research

RESULTS

C-C bond formation through β-diketones

Scheme 1. Reactions of β-dicarbonyl compound **14** with diphenylmethanol **1** catalysed by *N*-halo compound under **SFRC.**

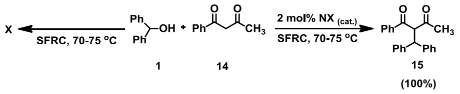

C-C bond formation through electron-rich C=C

Scheme 2. Direct coupling of diphenylmethanol **1** with 1,2-dihydronaphtene **16** catalysed by *N*-halo compounds under **SFRC.**

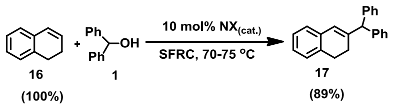

C-N bond formation

Scheme 4. Direct coupling of 1-(p-tolyl)ethan-1-ol **18** with acetonitrile catalysed by *N*-halo compound under **HCRC.**

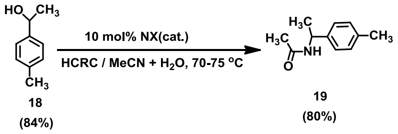

Scheme 5. Isothiocyanation of phenyl(p-tolyl)methanol **12** with (TMSNCS) catalysed by *N*-halo compound under **SFRC**.

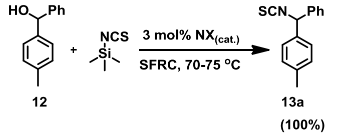

C-X bond formation

Table 1. Chlorination of various primary benzyl alcohols **6** with TMSCl catalysed by *N*-halo compound under **SFRC.**

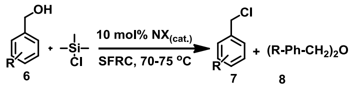

Entry	R	Conv. (%)[b] of 6	Relative distribution (%)[b]	
			7	8
1[c]	H (7a)	78	68	10
2	H (7a)	100	92	8
3[c]	3-CF_3 (7b)	/	/	/
4	3-CF_3 (7b)	91	79	12

[a] Reaction conditions: Benzyl alcohol **6** (0.5 mmol), TMSCl (0.55 mmol).
[b] Determined from ^1H NMR spectra of isolated crude reaction mixtures.
[c] In the absence of the catalyst.

C-O bond formation

Scheme 3. Transformation of diphenylmethanol **1** catalysed by *N*-halo compound under **SFRC** or **HCRC**.

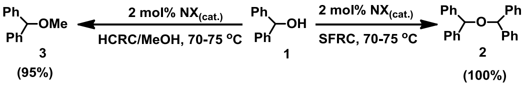

CONCLUSION

- We have introduced *N*-halo compounds as a new group of non-metal and non-acidic and environmentally friendly catalysts for comprehensive transformation of hydroxyl group with different nucleophile sources selectively and efficiently under **solvent-free reaction conditions** or **high substrate concentration reaction conditions**.
- The presented methodology is the new highly efficient and easy to perform approach to the synthesis of comprehensive type of derivatives starting from hydroxyl functional group targets and applying **solvent-free reaction conditions** or **high substrate concentration reaction conditions** as green chemical reaction protocol.

REFERENCES

[1] M. Jereb, D. Vražič, M. Zupan, *Tetrahedron,* , 67, 1355-1387, 2011
[2] M. Yasuda, S. Yamasaki, Y. Onishi, A. Baba, *Journal of the American Chemical Society,* 126, 7186-7187, 2004
[3] B. Blank, M. Madalska, R. Kempe, *Advanced Synthesis & Catalysis,* 350, 749-758, 2008
[4] R. Sanz, D. Miguel, A. Martínez, J. M. Álvarez-Gutiérrez, F. Rodríguez, *Organic Letters,* 9, 727-730, 2007
[5] H.-L. Yue, W. Wei, M.-M. Li, Y.-R. Yang, J.-X. Ji, *Advanced Synthesis & Catalysis,* 353, 3139-3145, 2011

Magnetic properties of nanoplatelet composite nanoparticles composed of hard-magnetic hexaferrite and soft-magnetic maghemite

Blaž Belec [1, 2], **Darko Makovec** [1, 2]
[1] Department of Material synthesis, Jožef Stefan Institute, Jamova cesta 39, Ljubljana, Slovenia
[2] Jožef Stefan International Postgraduate School, Jamova cesta 39, 1000 Ljubljana, Slovenia
blaz.belec@ijs.si

Magnetic properties of bi-magnetic sandwich-like composite nanoparticles, composed of a hard-magnetic barium hexaferrite ($BaFe_{12}O_{19}$) platelet core positioned in between two soft-magnetic spinel iron-oxide (maghemite, γ-Fe_2O_3) layers, will be presented. The composite nanoparticles were prepared with simple method based on co-precipitation of Fe^{3+}/Fe^{2+} ions in colloidal suspension of the core nanoparticles. The spinel formed exclusively as the layers at the core nanoparticles. The magnetic properties of the composite nanoparticles were measured using vibrating sample magnetometer perpendicular and parallel to their preferential magnetic orientation. For this purpose, the nanoparticles were hydrophobized with dodecylbenzene sulphonic acid (DBSa), dispersed in a hot liquid wax and magnetically oriented in a homogeneous magnetic field of 1T. The composite nanoparticles exhibit single-phase magnetic hysteresis, suggesting that the two phases are exchange coupled. The difference between in-plane and out-of-plane magnetic hysteresis showed some degree of magnetic orientation of the nanoparticles. The comparison between in-plane magnetic hysteresis of the core and the composite nanoparticles showed a large increase in saturation magnetization (M_S) and remanence (M_R), and decrease in coercivity (H_C) for the composite nanoparticles.

Magnetic properties of nanoplatelet composite nanoparticles composed of hard-magnetic hexaferrite and soft-magnetic maghemite

Blaž Belec[1,2] , Darko Makovec[1,2]

[1] Department for Material Synthesis – K8, Jožef Stefan Institute, Jamova cesta 39, 1000 Ljubljana, Slovenia
[2]Jožef Stefan International Postgraduate School, Jamova cesta 39, 1000 Ljubljana, Slovenia

blaz.belec@ijs.si ; *supervisor prof.dr. Darko Makovec

INTRODUCTION

- Composite nanoparticles combine at least two different materials in the one nanoparticle.
- Bi-magnetic composite nanoparticles combine two magnetically different materials.
- Interactions between the different magnetic phases can result in exchange interactions.

2 types of direct exchange interactions

Ferromagnetic + antiferro magnetic materials
- Extra source of anisotropy

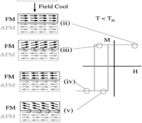

Magnetically hard + magnetically soft materials
- Improved energy product BH_{max}

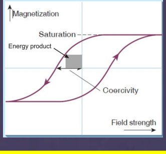

APPLICATION OF BI-MAGNETIC NANOPARTICLES

- Building blocks for permanent magnets with improved properties
- Exchange coupling effect could be applied to tune the properties of the materials for specific application

Magnetic hyperthermia

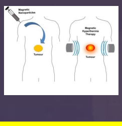

Permanent magnets

Recording and storage media

OUR WORK

- Analysis of magnetic properties of composite nanoparticles composed of hard-magnetic In- doped barium hexaferrite ($BaFe_{11.5}In_{0.5}O_{19}$) platelet core in between two soft-magnetic maghemite (ϒ-Fe_2O_3) layers.

PROBLEMS

- Magnetic properties of platelet nanoparticles depend on their orientation.
- Magnetic nanoparticles have to be magnetically oriented.

Requirement

Stable suspension of the nanoparticles in wax.

EXPERIMENTAL

Composite nanoparticles

- Co-precipitation of Fe^{3+}/Fe^{2+} in colloidal aqueous suspension of the hexaferrite core nanoparticles (A = 5,45 x 10 ^{18} nm^2) at 60 °C.

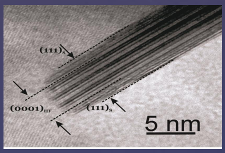

HREM image of the composite nanoparticle oriented edged-on with its large surface parallel to the electron beam.

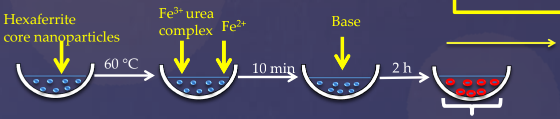

Composite nanoparticles

Adsorption of dodecylbenzene sulphonic acid and preparation of stable suspension

- Adsorption of DBSa in acidic medium at 100 °C.

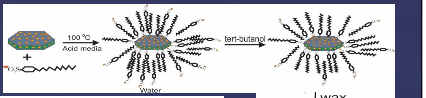

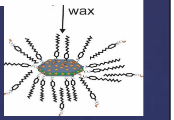

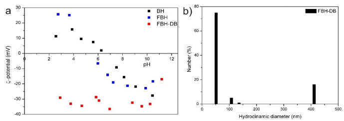

a) ζ-potential measurements of the nanoparticles in aqueous suspension and b) hydrodynamic diameter of the composite nanoparticles in tert-butanol.

MAGNETIC PROPERTIES

- Nanoparticles dispersed in a hot wax were magnetically oriented by exposure to the homogeneous magnetic field for 30 min.
- Solidified wax preserve the magnetic orientation of the nanoparticles.

Powder samples (not-oriented)

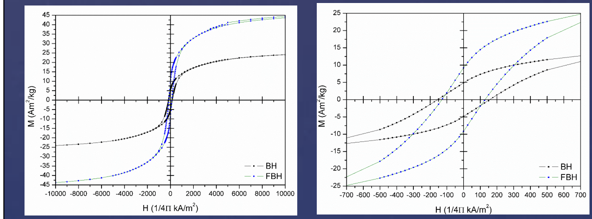

Comparison of the magnetic hysteresis of not-oriented hexaferrite core nanoparticles and composite nanoparticles.

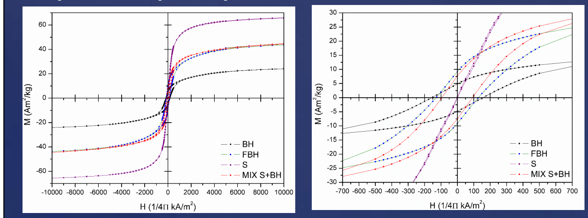

Comparison of the magnetic hysteresis of not-oriented hexaferrite core nanoparticles, maghemite nanoparticles, composite nanoparticles and physical mixture of hexaferrite and maghemite nanoparticles.

Magnetically oriented

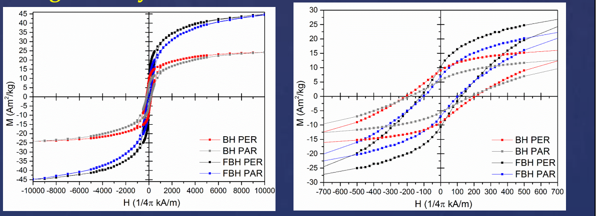

Comparison between the in-plane and out-of-plane magnetic hysteresis of hexaferrie core and composite nanoparticles.

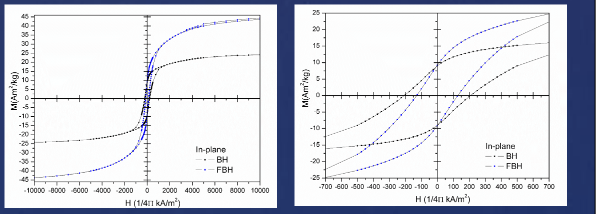

Comparison between the magnetic hysteresis of the in-plane oriented hexaferrie core and composite nanoparticles.

CONCLUSIONS

- Composite nanoparticles exhibit Increased M_S and M_R, and decreased H_C compare to the hexaferrite core nanoparticles due to the presence of the soft/magnetic maghemite layers.
- Comparison between magnetic hysteresis of the composite nanoparticles and mixture of hexaferrite core and maghemite nanoparticles suggest that the magnetically-different phases in the composite are direct-exchange coupled.

ACKNOWLEDGEMENT: This work was financially supported by ARRS. The authors acknowledge for the use of equipment in the CENN Nanocenter.

IPSSC: Microstructure, mechanical and electrical properties of Glass Fiber Reinforced Composites (GFRC)

Barbara Bertoncelj[1,2], Katarina Vojisavljević[3], Janez Rihtaršič[1], Gregor Jelenc[1], Barbara Malič[3]

[1] Domel, d.o.o., Železniki, Slovenia

[2] Jožef Stefan International Postgraduate School, Ljubljana, Slovenia

[3] Jožef Stefan Institute, Ljubljana, Slovenia
barbara.bertoncelj@domel.com

In this study, the influence of E-glass fiber and mineral filler content on the microstructure, physical, mechanical and dielectric properties of Glass Fiber Reinforced Composites (GFRC) was investigated. Five sets of GFRC, based on polymer resin with varying E-grade glass fibers and $CaCO_3$ mineral filler weight fractions (15/64, 20/59, 25/54, 30/49, 35/44), were commercially prepared. Test specimens were prepared by compression molding. Scanning Electron Microscope images revealed that at higher concentrations, the fibers clustered together, resulting in heterogeneous microstructures. Characterization of the composites showed that glass fiber content and distribution significantly affects the mechanical properties. The flexural strength of the composites decreased with increasing glass fiber content. The dielectric constant ε` decreased with increasing fiber content.

MEDNARODNA
PODIPLOMSKA ŠOLA
JOŽEFA STEFANA

JOŽEF STEFAN
INTERNATIONAL
POSTGRADUATE SCHOOL

Microstructure, mechanical and electrical properties of Glass Fiber Reinforced Composites (GFRC)

Barbara Bertoncelj[1,2], Katarina Vojisavljević[3], Janez Rihtaršič[1], Gregor Jelenc[1], Barbara Malič[3]
[1] Domel, d.o.o., Železniki, Slovenia
[2] Jožef Stefan International Postgraduate School, Ljubljana, Slovenia
[3] Jožef Stefan Institute, Ljubljana, Slovenia
Study program: Ecotechnology
Supervisor: prof. dr. Barbara Malič

Introduction

GFRC:

- replacement for traditional structural materials, such as steel and aluminium
- good dimensional stability, chemical and corrosion resistance and good insulating properties
- manufacturing process of products is energy less-consuming (such as injection moulding)
- applications are widespread in automotive, electronic and electro industry
- continuous improvement of properties and competitive price still makes them attractive for an even wider use

For example, typical products are internal automotive parts or assembling parts of electrical motors..

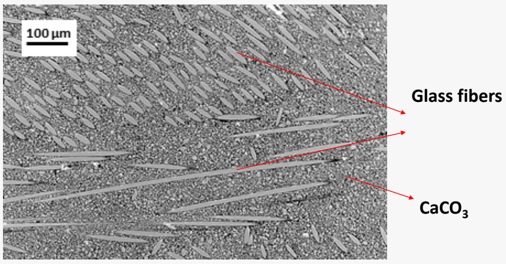

Physical and mechanical properties depend on the phase composition, physical and chemical properties of individual components and fiber distribution and orientation.

Aim of the work

To study the effect of **E-glass fiber** and **$CaCO_3$** mineral filler weight fraction on microstructure, physical, mechanical and electrical properties of composites.

Experimental work

Composition of GFRC samples.

	Polymer matrix	E-glass fibers	$CaCO_3$
	Content [wt.%]		
1	21	15	64
2	21	20	59
3	21	25	54
4	21	30	49
5	21	35	44

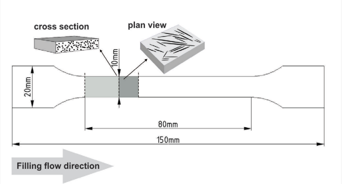

Scheme of the test specimen illustrating the cutting directions for cross-section and plane-view sections for SEM observation.

Results

Microstructure

plan-view section
cross section

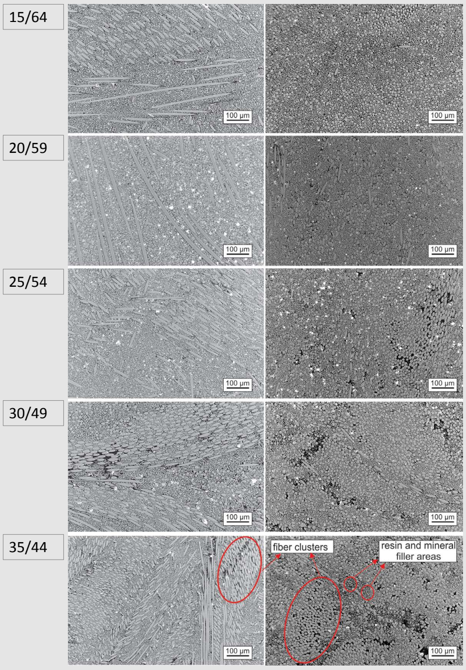

Density

Composition	Density [g/cm³]
15/64	2,04
20/59	2,03
25/54	2,02
30/49	2,04
35/44	2,03

Flexural strength

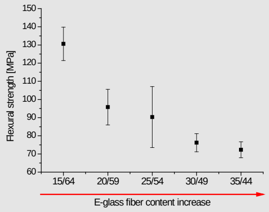

Flexural strength of GFRC samples.

Dielectric properties

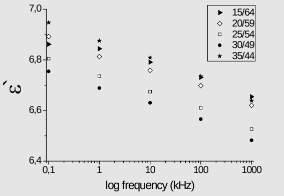

Frequency dependence of dielectric constant ε` for GFRC samples.

Conclusion

Density of GFRC samples did not change with the composition. SEM micrographs revealed that fiber distribution at lower weight fractions of EGF is quite homogeneous. With increasing EGF contents, above 25% wt., the distribution of the fibers becomes inhomogeneous. We connect the observed inhomogeneous microstructure with the deterioration of the flexural strength. The results showed that flexural strength of the composites decreased with increasing EGF content. The room temperature dielectric permittivity in all composites decreased with increasing frequency and with increasing glass fiber content.

Photogeneration of Charge Carriers in Few-Layer MoS_2

Tetiana Borzda[1,2], Christoph Gadermaier[1,2], Natasa Vujicic[1,3], Peter Topolovsek[1,2], Milos Borovsak[1], Tomaz Mertelj[1], Daniele Viola[4], C. Manzoni[4], E. A. A. Pogna[4], D. Brida[5], Maria Rosa Antognazza[6], Francesco Scotognella[6], Guglielmo Lanzani[6], Giulio Cerullo[4], and Dragan Mihailovic[1,2,7]

[1] Department of Complex Matter, Jozef Stefan Institute, Jamova 39, 1000 Ljubljana, Slovenia

[2] Jozef Stefan International Postgraduate School, Jamova 39, 1000 Ljubljana, Slovenia

[3] Institute of Physics, Bijenicka 46, 10000 Zagreb, Croatia

[4] Department of Physics, Politecnico di Milano, P. Leonardo da Vinci 32, 20133 Milan, Italy

[5] Department of Physics, University of Konstanz, PO box M696 78457 Konstanz, Germany

[6] Center for Nano Science and Technology, Italian Institute of Technology, Via Pascoli 70/3, 20133 Milano, Italy

[7] Center of Excellence in Nanoscience and Nanotechnology, Jamova 39, 1000 Ljubljana, Slovenia

tetiana.borzda@ijs.si

The two-dimensional semiconductor MoS_2 in its mono- and few-layer form is expected to have a significant exciton binding energy of several 100 meV, leading to the consensus that excitons are the primary photoexcited species. Nevertheless, even single layers show a strong photovoltaic effect and work as the active material in high sensitivity photodetectors, thus indicating efficient charge carrier photogeneration (CPG). Here we use continuous wave photomodulation spectroscopy to identify the optical signature of long-lived charge carriers and femtosecond pump-probe spectroscopy to follow the CPG dynamics. We find that intitial photoexcitation yields a branching between excitons and charge carriers, followed by excitation energy dependent hot exciton dissociation as an additional CPG mechanism. Based on these findings, we make simple suggestions for the design of more efficient MoS_2 photovoltaic and photodetector devices.

Photogeneration of Charge Carriers in Few-Layer MoS_2

Tetiana Borzda

Programme of study: Nanosciences and Nanotechnologies,
Department of Complex Matter, Jozef Stefan Institute
Jozef Stefan International Postgraduate School, Jamova 39, 1000 Ljubljana
MENTOR: doc. dr. Christoph Gadermaier

The subject of the research is dynamics of charge carriers in one- and few-layeres molybdenum disulfide (MoS_2);
The method of investigation is time-resolved optical spectroscopy;
The objects of research are layers of MoS_2.

Object of research

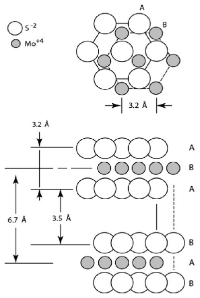

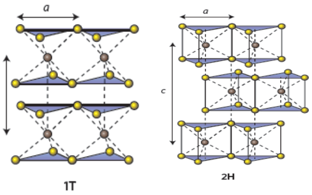

Schematic of the structural polytypes : 2H (hexagonal symmetry, two-layers per repeat units, trigonal prismatic coordination),
1T (tetragonal symmetry, one layer per repeat unit, octahedral coordination)

Samples

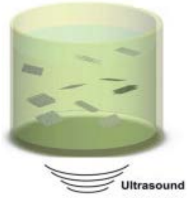

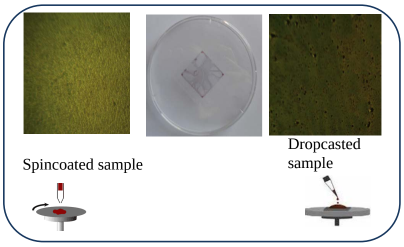

Optical characterization of MoS_2

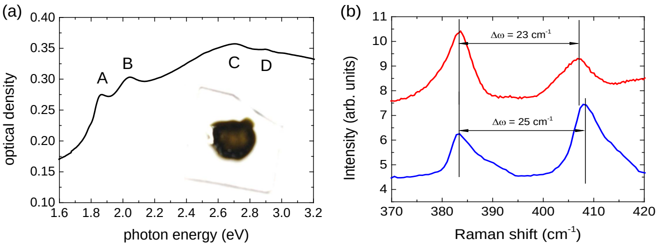

(a) Absorption spectrum of the sample of MoS_2 in PMMA. Inset shows a photograph (the dark area has a diameter of approximately 7-8 mm). (b) Raman spectra for two excitation wavelengths at 633 nm (red line) and 488 nm (blue line).

Method of time-resolved (pump-probe spectroscopy)

The basic idea of time-resolved (pump-probe) spectroscopy is to examine the temporal evolution of a system developing into and out of a non-equilibrium state.

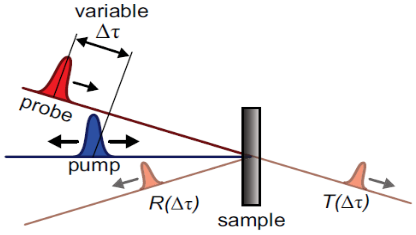

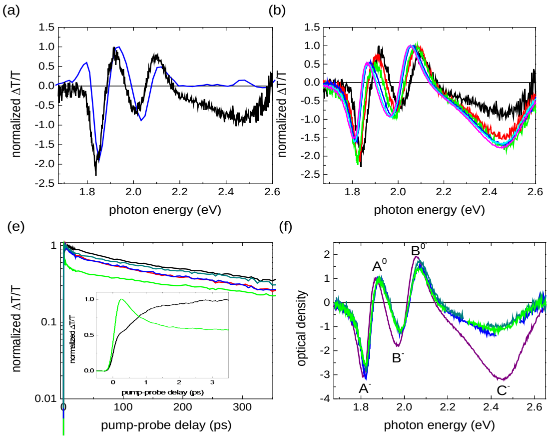

(a) Normalized cw photomodulation spectrum of MoS_2 in PMMA (blue) compared to the fs transient spectrum at 300 ps pump-probe (black) delay for 2 10^{14} cm^{-2} excitation fluence, 3.1 eV pump photon energy (b) pump-probe spectra at 300 ps normalized to the B exciton peak for different pump fluences at 3.1 eV pump photon energy: 2 (black), 3(red), 6 (green), 20 (blue), 40 (cyan) and 80 10^{14} cm^{-2} (e) normalized time traces for different probe energies: 2.48 (black), 2.25 (red), 2.07 (green), 1.94 (blue) and 1.80 eV (dark cyan) (f) normalized spectra at 300 ps pump-probe delay for different pump photon energies: 3.10 (purple), 2.48 (blue), 2.34 (dark cyan) and 2.25 eV (green).

Possible applying MoS_2 for photovoltaic application

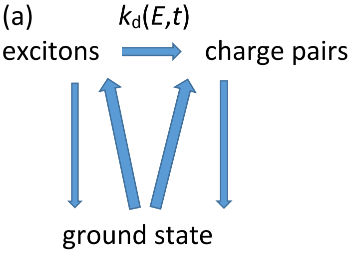
(a) $k_d(E,t)$

excitons → charge pairs

ground state

Non- destructive Analysis of Archaeological Metals

Helena Fajfar[1,2,3], **Zdravko Rupnik**[1], **Žiga Šmit**[1,4]
[1] Department of Low and Medium Energy Physics, Jožef Stefan Institute, Ljubljana, Slovenia
[2] Jožef Stefan International Postgraduate School, Ljubljana, Slovenia
[3] JUVI Domžale d.o.o., Domžale, Slovenia
[4] Faculty of Mathematics and Physics, University of Ljubljana, Ljubljana, Slovenia
helena.fajfar@ijs.si

Ion beam analysis is an efficient method for studies of archaeological metals. It is based on excitation of characteristic X-rays and gamma rays. In this paper we present PIXE and PIGE analysis of different metal alloys. Spot analysis was used for analysis of bronzes, which were used for medieval early fiery weapons. In the second part of the paper, the inhomogeneous metal objects are examined. The external beam facility was improved for the mapping measurements, which allow detection of inhomogeneous gilded layers. The new system allows the external beam to be scanned over an area of a few cm^2.

1 Introduction

Archaeological metals are important testimony of human past. Material identification is basic objective of scientific characterization of ancient objects and provides important clues about fabrication. Elemental analysis of metals provides valuable information about the composition of alloys and may lead to identifying the metal origin. Analytical data on metal composition may also provide interesting insight into past technologies, including mining, melting and metal working [1]. When a unique artefact is found, the analytical methods are required of being non-destructive and able to give the chemical analysis without sampling. PIXE and PIGE methods allow us detection of major, minor and trace elements. An advantage of PIXE compared to other IBA methods is its speed and sensitivity.

Non-destructive Analysis of Archaeological Metals

Helena Fajfar, uni. dipl. inž. kem. inž., Study programme: Ecotechnologia Jožef Stefan International Postgraduate School
Jožef Stefan Institute, Jamova cesta 39, 1000 Ljubljana, Slovenia
JUVI DOMŽALE d.o.o., Dragarjeva ulica 20, Rodica, 1230 Domžale, Slovenia
Mentor: prof. dr. Žiga Šmit, Jožef Stefan Institute, Jamova cesta 39, 1000 Ljubljana, Slovenia
Faculty of Mathematics and Physics, University of Ljubljana, Jadranska cesta 19, 1000 Ljubljana, Slovenia

INRODUCTION

The 2 MV particle accelerator at the Microanalytical Center of the Jožef Stefan Institute is equipped with four measuring lines. One line allows measurements with in-air proton beam. A major fraction of activity is devoted to the analysis of archaeological metals. Elemental analysis provides valuable information about the composition of alloys and may lead to identification of the metal origin. The external beam facility was improved for the mapping measurements. The recent metal analysis involves studies of bronzes which were used for fiery weapons. With the new system for mapping we analysed bronze ingots from prehistoric sites and detection of gilded layers in corroded objects.

Ion Beam Analysis

- frequently applied to the objects of cultural heritage
- non-destructive
- liquid, solid and powdered samples can be analyzed

PIXE

- Proton Induced X-ray Emission
- soft X-rays are absorbed
- very fast method
- highly sensitive
- unable to detect light elements
- detection limit for most el. is around 10 ppm

PIGE

- Proton Induced Gamma-ray Emission
- analysis deeper below surface
- able to detect light elements

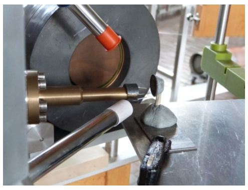

Figure 2: Measurement with in-air proton beam.

EXPERIMENTAL

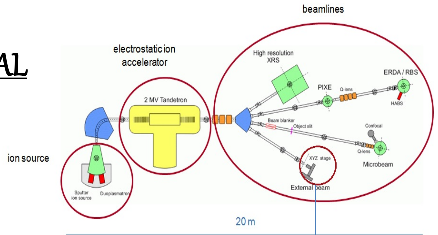

The new system for mapping allows the external beam to be scanned over an area of a few cm². The sample is fixed on a remote controlled stage driven by stepping motors. During the scanning process, the measurement process is executed through the following steps: moving the sample, data acquisition, saving the spectra, and moving to the next measuring point.

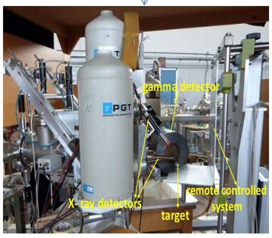

Figure 1: 2 MV Tandetron accelerator at MIC at Jožef Stefan Institute and the end station of the in-air beamline with the mapping system.

RESULTS

a) mapping

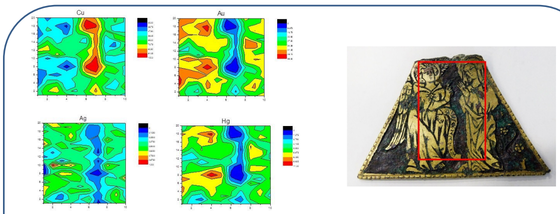

Figure 3: The Annunciation- fragment of a cross from the medieval period (14th-16th c.) Correlated maps of gold and mercury indicate that the method of amalgamation or fire gilding was applied. The scanning area was 10 x 20 mm.

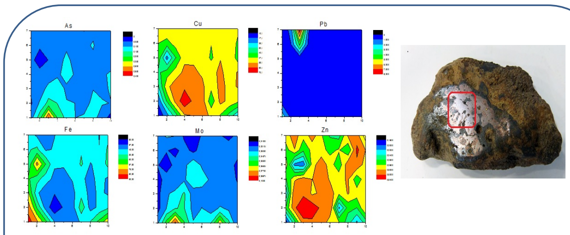

Figure 5: AES RUDE from Slovenia – a coarse alloy of copper and iron that circulated in the form of ingots in Italy during the 8th and 4th c. BC. It is believed it represented premonetary forms predating aes signatum and aes grave. The scanning area was 7 mm x 10 mm.

b) spot analysis

Table 1: Analysis of handgonnes (in mass %)

No/Location	Calib.[mm]	Fe	Ni	Cu	Zn	As	Ag	Sn	Sb	Pb
1 Čretež	25	0.15	0.37	82.0	0.71	0.61	0.14	3.95	2.66	9.46
2 Kostel	13	1.61	2.53	85.6	0.80	2.20	0.29	3.93	1.37	1.71
3 Šumberk	16	0.67	0.48	85.2	4.63	0.68	0.20	3.61	0.87	3.68

Figure 4: Fragments of three different handgonnes from south Slovenia.

CONCLUSION

Ion beam analysis are non-destructive methods. They are were useful for archaeological objects. With spot analysis three medieval weapons were measured. They are low quality, with large amounts of impurities. With new mapping system we can investigate a large area of the sample. The correlated maps on the fragment of medieval cross indicated that the method of amalgamation was applied.

Solution-derived Ta_2O_5 high-*K* thin films for gate dielectric applications

Raluca C. Frunză[1,2], Pedro Barquinha[3], Hermine Stroescu[4], Măriuca Gartner[4], Barbara Malič[1]

[1] Jožef Stefan Institute, Ljubljana, Slovenia

[2] Jožef Stefan International Postgraduate School, Ljubljana, Slovenia

[3] CENIMAT-I3N, Departament of Material Science and CEMOP/UNINOVA, Faculty of Science and Technology, Caparica, Portugal

[4] Ilie Murgulescu Institute of Physical Chemistry of the Romanian Academy, Bucharest, Romania

raluca.frunza@ijs.si

Ta_2O_5 is a promising high-*K* dielectric, due to its high refractive index, high dielectric permittivity (in the range 22-28 for the amorphous state) and good thermal and chemical stability. The present study reports the preparation of solution-derived Ta_2O_5 thin films processed at low temperatures suitable for applications in transparent electronics. The investigated thin films exhibited promising properties for capacitors and thin-film transistors.

Solution-derived Ta_2O_5 high-*K* thin films for gate dielectric applications

Raluca C. Frunză[1,2], **Pedro Barquinha**[3], **Hermine Stroescu**[4], **Măriuca Gartner**[4], **Barbara Malič**[1]
[1] Jožef Stefan Institute, Ljubljana, Slovenia
[2] Jožef Stefan International Postgraduate School, Ljubljana, Slovenia
[3] CENIMAT-I3N, Departament of Material Science and CEMOP/UNINOVA, Faculty of Science and Technology, Caparica, Portugal
[4] Ilie Murgulescu Institute of Physical Chemistry of the Romanian Academy, Bucharest, Romania

raluca.frunza@ijs.si

Introduction

A lot of effort has been put in the research and development of transparent thin-film transistors (TFTs), which are mainly used as on-off switches in active matrix backplanes of flat panel displays. Their main components are a semiconductor layer, three electrodes (gate, source and drain) and a dielectric layer, also referred to as the gate dielectric. All of them are deposited in form of thin films onto an insulator substrate. Ta_2O_5 is a promising high-*K* dielectric, due to its high refractive index, high dielectric permittivity (in the range 22-28 for the amorphous state) and good thermal and chemical stability. The present study reports the preparation of solution-derived Ta_2O_5 thin films processed at low temperatures suitable for applications in transparent electronics.

Experimental

Solution synthesis

The precursor for Ta_2O_5 thin films were prepared via alkoxide-based sol gel synthesis.

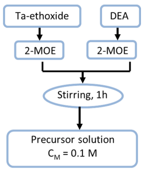

DEA = diethanolamine
2-MOE = 2-methoxyethanol

Thin film processing

- ❑ Substrates: $Pt(111)/TiO_2/SiO_2/Si$ (Pt/Si)
- ❑ Spin coating: 30 s, 3000 rpm
- ❑ Drying: 2 min at 150°C
- ❑ Pyrolysis: 2 min at 250°C, 300°C, 350°C, 400°C.

MIM structures

- ❑ sputtered Au/Cr top electrodes

TFT structures

- ❑ Substrate: Corning Eagle Glass
- ❑ Gate electrode: sputtered IZO, lift-off
- ❑ Dielectric: spin-coated Ta_2O_5 (≥ 250 nm), dry-etching
- ❑ Semiconductor: sputtered GIZO, lift-off
- ❑ Source-drain electrodes: e-beam evaporated Ti/Au, lift-off
- ❑ Annealing: 200 °C, air, 1h

IZO = indium zinc oxide
GIZO = gallium indium zinc oxide

Results

Compositional analysis

- ❑ All samples were XRD-amorphous, consistent with the low processing temperatures.

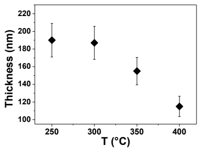

Thickness values as estimated from FE-SEM cross-section images.

- ❑ Asylum Research (MFP-3D-S™) atomic force microscope (AFM)

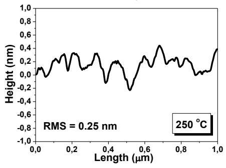

AFM surface profile of the 250 °C samples.

- ❑ The samples had smooth and flat surfaces with root-mean-square (RMS) vertical roughness values up to 0.3 nm.

- ❑ Perkin Elmer Spectrum 100 Fourier-transform infrared (FT-IR) spectrometer

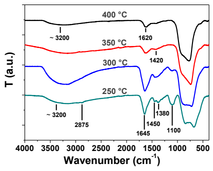

Band (cm^{-1})	Groups
3200	O-H, N-H, H_2O
1620-1645	N-H, C=N, H_2O
1420-1450	C-H
1380	C-H
1100	C-C, C-O
< 1000	Ta-O

FT-IR spectra of the Ta_2O_5 thin films prepared on Pt/Si.

- ❑ Residues of functional groups remained in the films upon heating to 250 °C, and they could be detected in a much lower amount upon heating to 400 °C.

Optical properties

- ❑ UV-Vis Variable Angle Spectroscopic Ellipsometer with rotating analyzer from J.A. WOOLLAM
- ❑ In accordance with the densification taking place at higher heating temperatures, the refractive index ranged from 1.7 to 1.99 for the processing temperatures in the range 250–400 °C.

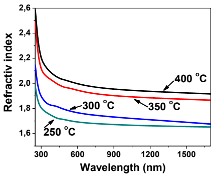

Refractive index dispersion of the thin films, as recorded by spectroscopic ellipsometry

Electrical properties, MIMs on Pt/Si

- ❑ Measurements at room temperature
- ❑ HP 4284A Impedance analyzer
- ❑ 50 mV, 100 kHz
- ❑ The permittivity (ε) values increased with processing temperature.
- ❑ All samples exhibited dielectric losses (tan δ) up to 6% at 100 kHz.
- ❑ Keithley 2602A system sourcemeter and HP 16058A test fixture
- ❑ The leakage currents also proved to be dependent on the thermal budget of the samples.

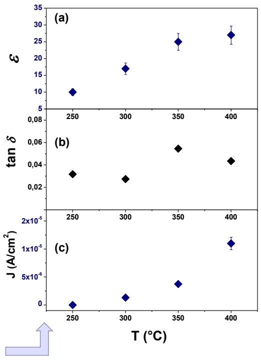

Electrical properties of the Ta_2O_5 thin films as a function of the processing temperature: (a) dielectric permittivity and (b) loss factor at 100 kHz, and (c) leakage current density at the applied field of 160 kV/cm.

Transfer characteristics, TFTs

- ❑ Keithley 4200-SCS and Janis ST-500
- ❑ Higher field-effect mobility - μ_{FE} (hence, on-current) and more negative turn-on voltage with 350 °C.

Transfer characteristics obtained at V_D = 1V. The extracted values of on/off ratio, subthreshold swing (S) and μ_{FE} are given in the table below.

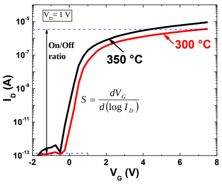

Dielectric	On/Off	S (V/dec)	μ_{FE} (cm^2/Vs)
300 °C	1.9 x 10^8	0.17	16.1
350 °C	4.6 x 10^8	0.17	21.1

Conclusions

Solution-derived Ta_2O_5 thin films were processed at temperatures not exceeding 400 °C. The amorphous thin films exhibited smooth and flat surfaces with low average roughness values. Higher processing temperatures rendered better properties in terms of densification and the removal of organics. The samples processed at higher temperatures exhibited higher permittivity values. The film processed at 400 °C exhibited the permittivity value of 27± 2. Yet, the leakage currents increased with the heating temperature. TFTs with the solution-derived gate insulators and sputtered GIZO channel layer rendered good operating properties, such as *on/off* ratios $>10^8$ and $\mu_{FE}>10$ cm^2/Vs, with slight improvements obtained in the case of the processing temperature of 350 °C. Therefore, the investigated Ta_2O_5 thin films exhibited promising properties for both passive and active electronic devices.

Matrix degradation as a mechanism for nanoparticles release from food contact materials

Viviana Golja[1,2], Goran Dražić[2,3,4], Martina Lorenzetti[4], Maša Zalaznik[5], Mitjan Kalin[5], Saša Novak[2,4]

[1] National Institute of Public Health, Ljubljana, Slovenia

[2] Jožef Stefan International Postgraduate School, Ljubljana, Slovenia

[3] Laboratory for Materials Chemistry, National Institute of Chemistry, Ljubljana, Slovenia

[4] Department of Nanostructured Materials, Jožef Stefan Institute, Ljubljana, Slovenia

[5] Laboratory for Tribology and Interface Nanotechnology, Faculty of Mechanical Engineering, University of Ljubljana, Slovenia

Viviana.Golja@nijz.si

Materials in contact with foodstuffs may contain nanoparticles which improve their properties. However, transfer of nanoparticles from the material into foodstuffs is not desirable. When nanoparticles are embedded in the matrix, probability of transfer is small, but release can be promoted by matrix degradation. Matrix degradation of quasi-ceramic coating on commercially available pans was studied. The most probable mechanisms of degradation were identified as mechanical, thermal and chemical. Our results show that matrix degradation during the worst case conditions of use may cause particles release into foodstuffs.

MEDNARODNA
PODIPLOMSKA ŠOLA
JOŽEFA STEFANA

JOŽEF STEFAN
INTERNATIONAL
POSTGRADUATE SCHOOL

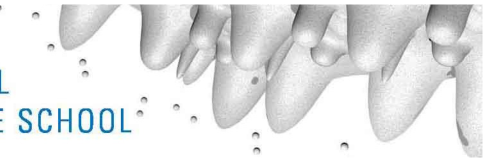

MATRIX DEGRADATION AS A MECHANISM FOR NANOPARTICLES RELEASE FROM FOOD CONTACT MATERIALS

Viviana Golja[1,2], Goran Dražić [1,3,4], Martina Lorenzetti [4], Maša Zalaznik [5], Mitjan Kalin [5], Saša Novak [1,4]

[1]Jožef Stefan International Postgraduate School,Ljubljana, Slovenia
[2]National Institute of Public Health,Ljubljana, Slovenia
[3]National Instutute of Chemistry,Ljubljana, Slovenia
[4]Jožef Stefan Institute, Ljubljana, Slovenia
[5]Faculty of mechanical Engineering, Ljubljana, Slovenia

Food contact material: pan with non-stick coating containing nanoparticles (silicone matrix with embedded TiO_2 and SiO_2 particles)

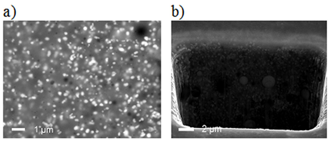

Figure 1: (a) Microstructure of the coating surface observed by FE SEM and
(b) cross- section observed by FIB SEM

►Possible issue: RELEASE of nanoparticles into food by matrix degradation

CHEMICAL DEGRADATION

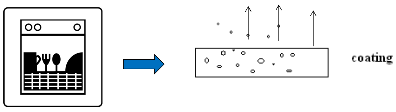

THERMAL DEGRADATION

DSC/TG examination: NETZSCH STA 449 C/6/G Jupiter – QMS 403, Germany during heating up to 700 °C, with a rate of 10 °C /min.

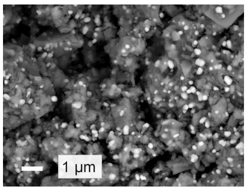

Figure 2: Scanning electron micrograph of the coating after heating at 700 °C

MECHANICAL DEGRADATION

► Scratch testing

Revetest scratch tester CSM Instruments RST S/N 01-04283, Switzerland
progressively increased load from 1 N to 30 N
rate 93,10 mm/min, scratch length 3 mm

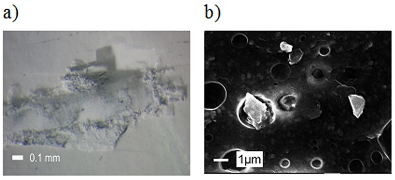

Figure 3: (a) Low magnification image of the scratch and (b) SEM image of the formed particles

► Wear testing

Tribometer - UMT-2, CETR, CA, USA
Reciprocating sliding, ceramic (Al_2O_3) pin
Load: 3 N, Frequency: 3 Hz,Sliding velocity: 0.03 m/s, Stroke: 5 mm

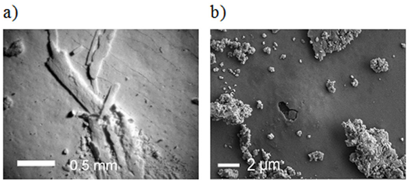

Figure 4: (a) Debris after wear test: stereomicroscope image and (b) SEM micrograph

RESULTS Nanoparticles may be released into food after matrix degradation

KNOWLEDGE CAN BE USED FOR

►**RISK ASSESSMENT** according to efsa document: Guidance on the risk assessment of the application of nanoscience and nanotechnologies in the food and feed chain EFSA Journal 2011;9(5):2140

The authors would like to thank Dr. N. Drnovšek for SEM imaging, Dr. M. Maček for DSC/TG analysis and Dr. S. Paskvale for scratch testing

Controlling the composition of electrodeposited Fe-Pd nanowires and thin films via determination of the diffusion and electrode kinetic parameters

Nina Kostevšek[1,2], Darja Pečko[1], Boris Pihlar[3], Spomenka Kobe[1], Kristina Žužek Rožman[1]

[1] Department for nanostructured materials, Jožef Stefan Institute, Ljubljana, Slovenia

[2] Jožef Stefan International Postgraduate School, Ljubljana, Slovenia

[3] Faculty of Chemistry and Chemical Technology, University of Ljubljana, Ljubljana, Slovenia

nina.kostevsek@ijs.si

Fe-Pd alloys have many potential applications because of their unique chemical and magnetic properties, which can be tailored by changing their composition. We have investigated the kinetic parameters for depositing Fe and Pd and their influence on the Fe-Pd alloy's composition, while performing the deposition on a flat Au electrode and into an Au-sputtered porous alumina template. The electrodeposition of Fe and Pd was found to be irreversible and diffusion-controlled. The diffusion coefficient was found to be lower for both metallic ions, by 2-3 times, when the template was used as a working electrode. However, the exchange current densities are comparable for Fe^{2+} and Pd^{2+} on both working electrodes. This indicates that the kinetics of the electrodeposition process is not influenced by the electrode geometry. Because of similar diffusion-coefficient ratios and similar kinetics on both the investigated working electrodes, using the same deposition conditions results in Fe-Pd-based thin films and nanowires having similar compositions.

Controlling the composition of electrodeposited Fe-Pd nanowires and thin films via determination of the diffusion and electrode kinetic parameters

Nina Kostevšek[1,3], Darja Pečko[1], Boris Pihlar[2], Spomenka Kobe[1], Kristina Žužek Rožman[1]

[1] Department for nanostructured materials, Jožef Stefan Institute, Ljubljana, Slovenia
[2] Faculty of Chemistry and Chemical Technology, University of Ljubljana, Ljubljana, Slovenia
[3]Jožef Stefan International Postgraduate School, Ljubljana, Slovenia
Programme: Nanosciences and Nanotechnologies, Mentor: doc. dr. Kristina Žužek Rožman

Introduction

Why Fe Pd alloy?

Unique chemical and magnetic properties, which can be tailored by changing their composition

→ SEVERAL APPLICATIONS:

- Alloy composition **28-31 at.% of Pd - shape memory effect**
- Alloy with about **50 at.% of Pd** represent promising candidates for micro-electro-mechanical systems (MEMS) due to their high magnetocrystalline anisotropy
- **Pd-rich alloys** exhibit catalytic properties, which can result in a high hydrogen-adsorption capacity

Why electrochemical synthesis?

Cost-effective and simple method to prepare metals alloys with different geometries:

- **Thin films:** flat electrode as working electrode
- **Nanowires/nanotubes**: porous alumina template (200 nm pore diameter) as working electrode

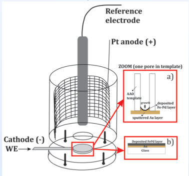

Aim of this study:

Understanding and comparing the diffusion and kinetics of the same process at working electrodes with different geometries to optimize the synthesis procedure!

Electrochemical study

Electrolyte composition

$c\ ((NH_4)_2C_6H_6O_7) = 0.4\ M$
$c\ (FeCl_3) = 200\ mM$
$c\ (PdCl_2) = 30\ mM$
$c(NH3)= 1M$
pH = 9, T = 25 °C

Fe^{3+}-citrate complex
$[Pd(NH_3)_4]^{2+}$ complex

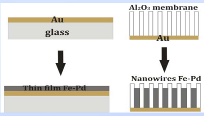

Linear diffusion at flat and porous alumina electrode!

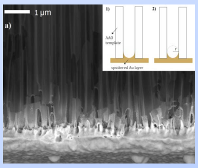

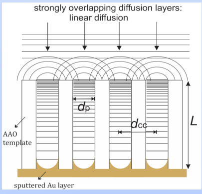

1. Cyclic voltammetry study of single Fe and Pd electrolytes to index reduction and oxidation reactions (peaks) !

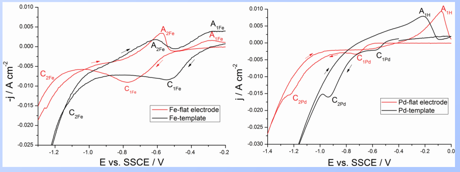

2. Peak position in the common Fe-Pd electrolyte differ from the position in the single metal electrolyte!

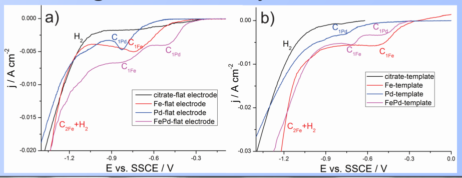

3. Calculations

If dependence of the peak current against square root of scan rate is linear, then the **diffusion coefficient** can be calculated from **Randles-Sevcik equation**:

$$i_p = 2{,}99 \cdot 10^5\, \alpha^{1/2}\, n^{3/2}\, A\, D_0^{1/2}\, C_0^*\, \nu^{1/2}$$

Charge transfer coefficient α can be determined by using **Delahay equation**:

$$|E_p - E_{p/2}| = \frac{1{,}857\, R\, T}{\alpha\, n_\alpha\, F}$$

Butler-Volmer analysis at low overpotentials was performed, where the **Butler-Volmer equation** can be used to calculate **exchange current density**:

$$j = j_0 \frac{F}{RT} \eta$$

Three important data from CVs: peak position (voltage $\mathbf{E_p}$), peak position at half height ($\mathbf{E_{p/2}}$) and peak height (current $\mathbf{i_p}$)!

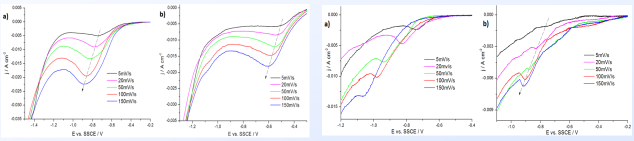

Fe on flat electrode
Fe on porous AAO electrode
Pd on flat electrode
Pd on porous AAO electrode

Ion	Electrode	α	*D* (cm²/s)	j_o (A cm⁻²)
Fe^{3+}	Flat electrode	0.46 ± 0.05	(2.1 ± 0.1)x10⁻⁵	(1.1±0.1)x10⁻⁴ ($Fe^{2+} \rightarrow Fe^0$)
Fe^{3+}	Template	0.63 ± 0.05	(0.7 ± 0.1)x10⁻⁵	(1.5±0.1)x10⁻⁴ ($Fe^{2+} \rightarrow Fe^0$)
Pd^{2+}	Flat electrode	0.42 ± 0.05	(5.1 ± 0.1)x10⁻⁵	(1.2±0.1)x10⁻⁴ ($Pd^{2+} \rightarrow Pd^0$)
Pd^{2+}	Template	0.35 ± 0.05	(2.7 ± 0.1)x10⁻⁵	(1.4±0.1)x10⁻⁴ ($Pd^{2+} \rightarrow Pd^0$)

4. Electrodeposition of Fe-Pd nanowires and thin films at different applied potentials

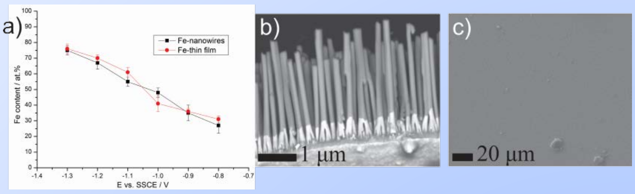

Graph indicating the influence of the cathodic potential on the Fe content in the Fe-Pd alloy in nanowires and in thin films(a), SEM images of b) **Fe-Pd nanowires** after AAO template removal and c) **Fe-Pd thin film** at -1.2 V.

Conclusions

- The electrodeposition of Fe and Pd is a irreversible and diffusion-controlled process
- The diffusion coefficient is found to be higher on the flat electrode for both investigated ions, due to the hindered mass transport in long non-conductive AAO pores
- $D_{Pd} > D_{Fe}$ for both electrodes
- Exchange current densities j_o for Fe^{2+} and Pd^{2+} are very similar for the flat electrode and in the template → the geometry of the electrode has no significant influence on the rate of the deposition reaction
- An almost equal alloy composition of thin films and nanowires was obtained when the same deposition conditions were used due to the comparable kinetics for both ions and the similar diffusion coefficients ratios $\frac{D_{Fe}}{D_{Pd}}$ for both working electrodes

Understanding the diffusion and kinetic parameters of the electrochemical deposition process allow us to fabricate Fe-Pd alloy with different shapes (thin films, nanowires) and, at the same time, precisely control the composition!

Acknowledgement: This work was supported by Slovenian Research Agency (ARRS) via J2-4316 project.

nina.kostevsek@ijs.si

Inkjet printing of alkoxide-based precursor solution for use in transparent electronics

Aleksander Matavž[1,2], Raluca C. Frunză[1], and Barbara Malič[1]
[1] Jožef Stefan Institute, Electronic Ceramics Department, Ljubljana, Slovenia
[2] Jožef Stefan International Postgraduate School, Ljubljana, Slovenia
matawzh@gmail.com

We have studied the fabrication of inkjet-printed, a few 10 nm thick 2D-structures of a Ta_2O_5-based dielectric for possible use in transparent electronics. The precursor solution, consisting of Ta-, Al-, and Si-alkoxides dissolved in 2-methoxyethanol and ethanol, was modified in terms of viscosity and surface tension to be suitable for piezoelectric inkjet printing. The viscosity of the solution was increased by admixing a more viscous solvent, i.e. glycerol. The as-prepared ink was stable and jetting even after long periods of time. We adjusted the printing parameters to achieve the best patterning quality on indium tin oxide (ITO) covered glass substrates. The functional properties of the inkjet-printed layers were compared to the state-of-the-art spin-coated films.

Inkjet printing of alkoxide-based precursor solution for use in transparent electronics

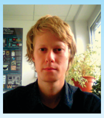

Aleksander Matavž [1,2], Raluca C. Frunză [1], and Barbara Malič [1]

[1]Jožef Stefan Institute, Slovenia, [2]JSI Postgraduate School, Slovenia

E-mail: matawzh@gmail.com

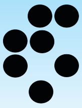

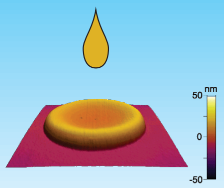

INTRODUCTION

The global trend to decrease the fabrication costs and waste production has promoted the development of direct pattering techniques, such as inkjet printing. Here, we report on the inkjet-printed Ta_2O_5-based dielectric structures for potential use in transparent electronics. In inkjet printing, the target values of viscosity and surface tension of the ink should be met. The proposed solution-based approach allowed us to print structures with thicknesses of a few tens of nanometers.

EXPERIMENTAL

Ta_2O_5-based solution

Alkoxide-based sol-gel precursor solutions (c = 0.1 M) of the ternary composition $Ta_2O_5 – Al_2O_3 – SiO_2$ with the Ta:Al:Si = 8:1:1 atomic ratio, further denoted as TAS.

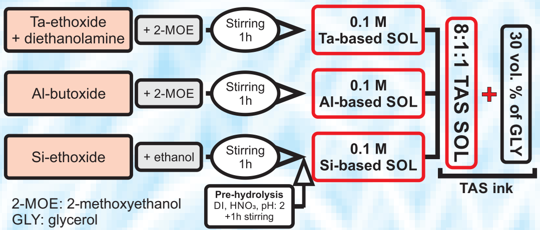

2-MOE: 2-methoxyethanol
GLY: glycerol
DI: deionized water

- Inkjet printing (TAS ink)
  - Dimatix DMP 2831
  - 1, 2, and 3 layers
- Spin-coating (TAS sol)
  - 5 layers (25 nm)
  - 10 layers (55 nm)
- Heat treatment
  - drying: 10 min / 150°C
  - heating: 10 min / 350°C
- Rheometer
  - Physica MCR 301
- Surface tension
  - KRÜSS EasyDrop DSA20E

- ITO-coated glass substrates
- Profilometer
  - Bruker Dektak XT
- Scanning electron microscopy
  - JEOL Ltd. JSM-7600F
- Atomic force microscopy (AFM)
  - Asylum Research MFP-3D-SA™
- Impendance analyzer
  - HP 4284A
- Leakage current
  - Aixacct TF 2000E

RESULTS

For stable drop formation, viscous (Re) and surface tension forces (We) have to be in balance. The Z number expresses the ratio between these forces. The ink had the physical properties suitable for inkjet printing.

$$Z = \frac{Re}{\sqrt{We}} = \frac{\sqrt{a\rho\gamma}}{\eta}$$

- a - nozzle diameter
- ρ - density
- γ - surface tension
- η - dynamic viscosity

Printable range: $1 < Z < 10$ [1]

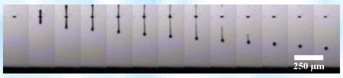

- $\eta = 10.1$ mPa s
- $\gamma = 32.9$ mN m^{-1}
- Nozzle diameter: 21.5 µm
- Amplitude: 21 V
- Jetting frequency: 20 kHz

$Z_{calc} = 3$

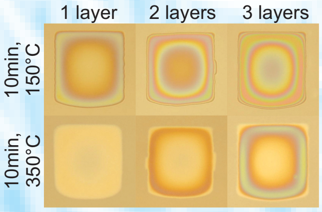

An array of squares with dimensions of 500 x 500 µm^2 was printed onto ITO-coated glass substrates. We investigated structures consisting of 1, 2, and 3 printed layers.

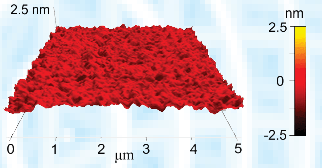

The samples exhibited very smooth, uniform and defect-free surfaces with the surface roughness lower than **0.5 nm**.

The coffee stain effect was more pronounced for 2 and 3 inkjet-printed layers. The thickness of 1 printed layer, heated at 350°C was **~40 nm**.

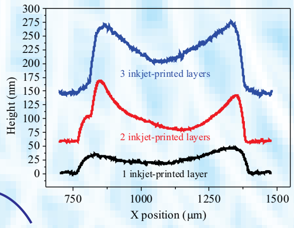

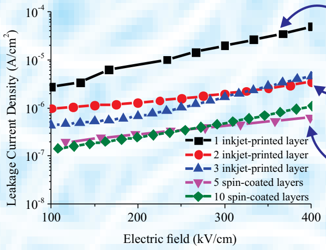

Poor performance of 1 inkjet-printed layer.

Reliable performance of 2 and 3 printed layers.

The best performance of spin-coated samples

Inkjet-printed samples had dielectric constant comparable to spin-coated samples. The dielectric losses decreased with increasing number of layers.

	Dielectric constant	Dielectric losses
1 inkjet-printed layer	**15** ± 2	**0.18** ± 0.06
2 inkjet-printed layers	**16** ± 2	**0.16** ± 0.06
3 inkjet-printed layers	**15** ± 2	**0.05** ± 0.01
5 spin-coated layers	**17** ± 2	**0.14** ± 0.03
10 spin-coated layers	**16** ± 2	**0.04** ± 0.01

Main observations

- All layers were smooth and without evident defects.
- 2 and 3 printed layers had a larger coffee stain effect.
- Good el. performance of 2 and 3 inkjet-printed layers.

CONCLUSIONS

We successfully inkjet-printed dielectric layers. The surface of structures was flat and smooth. The fabricated structures consisted of up to three layers of tantalum-based dielectric. The structure consisting of 1 inkjet-printed layer had poor leakage properties. The electrical properties were improved for 2 or 3 layered structures, and comparable to the properties of spin-coated films.

Literature and acknowledgements

We would like to thank Aljaž Drnovšek for profilometry measurements and to the Centre of Excellence NAMASTE and NANOCENTER, for providing their equipment. We acknowledge the financial support of the Slovenian Research Agency (J2 4273, P2-0105).

[1] Derby, B.; J. Eur. Ceram. Soc. 2011, 31, 2543-2550

Amino-acid-iron-oxide-nanoparticles: adsorption studies and colloidal properties

Klementina Pušnik[1,2], Gregor Marolt[3], Sašo Gyergyek[1], Darko Makovec[1,2,]
[1] Department for Materials Synthesis, Jožef Stefan Institute, Ljubljana, Slovenia
[2] Jožef Stefan International Postgraduate School, Ljubljana, Slovenia
[3]Faculty of Chemistry and Chemical Technology, Ljubljana, Slovenia
klementina.pusnik@ijs.si

For majority of different applications of superparamagnetic iron-oxide nanoparticles in medicine and technology, stable aqueous suspensions are required. One possible type of nontoxic and biocompatible molecules used in the stabilization of aqueous nanoparticles suspensions are amino acids. In this work the adsorption of aspartic amino acid (ASP) onto the iron-oxide nanoparticles and the colloidal properties of their aqueous suspensions were studied. Even the ASP-adsorbed nanoparticles display moderate zeta potential; they form the colloidally-stable aqueous suspensions. Direct analysis of ASP in the supernatant of the ultracentrifuged suspensions using an ion chromatography with pulsed amperometric detection suggested adsorption of the ASP in the form of large molecular associates, sterically stabilizing the suspensions.

Amino-acid-iron-oxide-nanoparticles: adsorption studies and colloidal properties

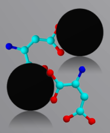

Klementina Pušnik[1,2], Gregor Marolt[3], Sašo Gyergyek[1], Darko Makovec[1,2,]
[1] Department for Materials Synthesis, Jožef Stefan Institute, Ljubljana, Slovenia
[2] Jožef Stefan International Postgraduate School, Ljubljana, Slovenia
[3]Faculty of Chemistry and Chemical Technology, Ljubljana, Slovenia

INTRODUCTION

For majority of different applications of superparamagnetic iron-oxide nanoparticles in medicine and technology, stable aqueous suspensions are required. One possible type of nontoxic and biocompatible molecules used in the stabilization of aqueous nanoparticles suspensions are amino acids. In this work the adsorption of aspartic amino acid (ASP) onto the iron-oxide nanoparticles and the colloidal properties of their aqueous suspensions were studied. Even the ASP-adsorbed nanoparticles display moderate zeta potential; they form the colloidally-stable aqueous suspensions. Direct analysis of ASP in the supernatant of the ultracentrifuged suspensions using an ion chromatography with pulsed amperometric detection suggested adsorption of the ASP in the form of large molecular associates, sterically stabilizing the suspensions.

EXPERIMENTAL SECTION AND RESULTS

- Precipitation of Fe^{3+} and Fe^{2+} ions from their aqueous solutions with aqueous ammonia to synthesize maghemite nanoparticles,

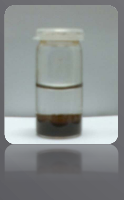

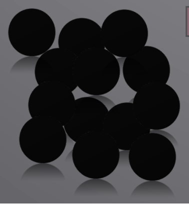

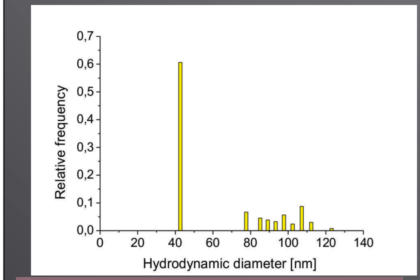

Particles size distribution of aspartic-acid-adsorbed iron-oxide nanoparticles in aqueous suspension (5 mg/mL).

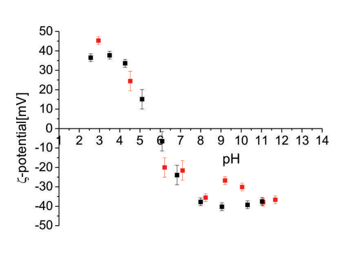

ζ-potential of: iron-oxide nanoparticles (black dots), aspartic-acid adsorbed-iron-oxide-nanoparticles (red dots).

- Amino acid was adsorbed onto the synthesized nanoparticles at pH=4.0,

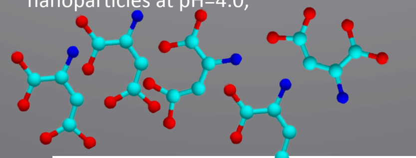

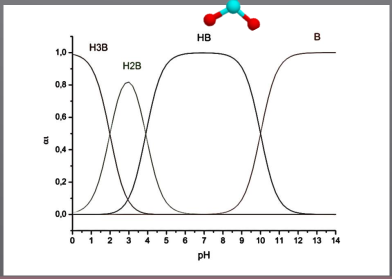

Calculated curves showing relative fraction of individual ASP species as a function of pH (marked in the graph with H3B, H2B, HB, B for undissociated, one carboxyl group dissociated, two carboxyl groups dissociated, amino group deprotonated, respectively).

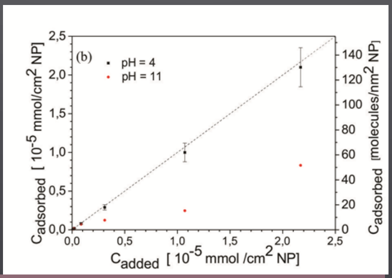

Adsorption isotherm of ASP at pH=4 and pH=11

- Amino-acid-adsorbed iron-oxide nanoparticles were dispersed in water at pH=11.

Aspartic-acid adsorbed-iron-oxide nanoparticles suspensions (5 mg/mL).

Schematic presentation of aspartic acid adsorption onto iron-oxide nanoparticles in the form of molecular associates .

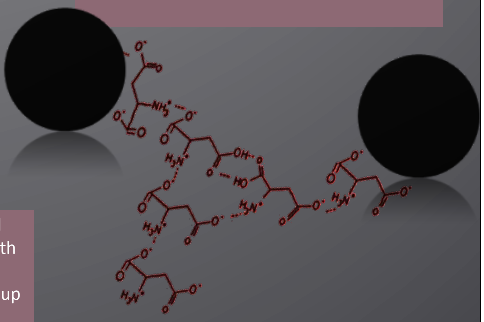

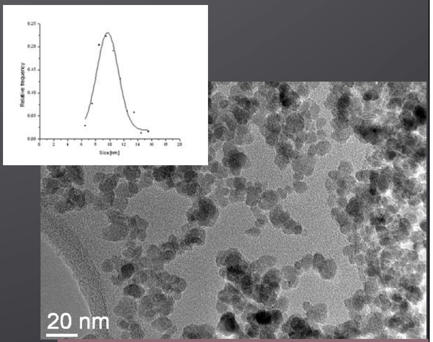

TEM image and the corresponding size distribution of iron-oxide nanoparticles (γ-Fe_2O_3).

CONCLUSIONS

The adsorption of aspartic acid (ASP) on the iron-oxide (maghemite) nanoparticles in aqueous suspension does not change their zeta potential significantly. There is no change in izo-electric point and the absolute values of the zeta potential remained relatively low. However, even the absolute values of zeta potential were low; the suspension of the ASP-adsorbed nanoparticles at basic pH was relatively stable. The adsorption curves measured by direct analysis of ASP in the supernatant of the ultracentrifuged suspensions using an ion chromatography with pulsed amperometric detection suggested that the adsorption of the ASP does not follow an adsorption isotherm. Very high concentrations of the ASP attached onto the nanoparticles suggests that the ASP is adsorbed in the form of large molecular associates, which sterically contribute to stabilization of the suspension.

ACKNOWLEDGEMENT

This work was financially supported by ARRS. The authors acknowledge the use of equipment in the Center of Excellence on Nanoscience and Nanotechnology–Nanocenter.

Selectivity in the Synthesis of Unsymmetrical Tetraoxanes

Katarina Starkl[1,2], **Jernej Iskra**[1]
[1] Department of Physical and Organic Chemistry (K-3), Jožef Stefan Institute, Ljubljana, Slovenia
[2] Jožef Stefan International Postgraduate School, Ljubljana, Slovenia
katarina.starkl@ijs.si

Unsymmetrical tetraoxanes are representatives of synthetic cyclic peroxides which evolved from artemisinin, a natural product used in the first-line treatment for malaria and a promising antitumor, antiparasitic and antiviral agent. Tetraoxanes might exhibit enhanced antimalarial activity due to two peroxide groups in the molecule that are essential for bioactivity of cyclic peroxides. Chemical synthesis of unsymmetrical 1,2,4,5-tetraoxanes could be straightforward with acid-catalysed cyclization of *gem*-dihydroperoxide and ketone, however problems with formation of various side-products hampers their development. We have studied the cyclization of cyclic *gem*-dihydroperoxides and various ketones in order to develop a general method for synthesis of unsymmetrical tetraoxanes was developed with an emphasis on selectivity of tetraoxanes. The method was adopted for the synthesis of various 1,2,4,5-tetraoxanes which will be evaluated for in-vitro antibacterial and antitumor activity.

MEDNARODNA
PODIPLOMSKA ŠOLA
JOŽEFA STEFANA

JOŽEF STEFAN
INTERNATIONAL
POSTGRADUATE SCHOOL

Selectivity in the Synthesis of Unsymmetrical Tetraoxanes

Katarina Starkl[a,b], Jernej Iskra[a]
Mentor: Jernej Iskra
[a] "Jožef Stefan" Institute, Department of Physical and Organic Chemistry (K3), [b] Jožef Stefan International Postgraduate School, study programme: Nanosciences and nanotechnologies

Peroxides as therapeutical agents

Natural products containing peroxide groups exhibit broad spectrum of bioactivity but they have not been fully exploited as therapeutic agents due to their low availability.[1] Artemisinins are one of the most important representative and are recommended as the first-line treatment for malaria for more than a decade. Beside antiparasitic activity, artemisinins exhibit also antitumor, antiviral, antibacterial and anti-inflammatory activity, for which an endoperoxidic group is essential.[2] Simplification of artemisinin structure, needed to facilitate the production and to improve pharmacokinetic properties, resulted in development of synthetic cyclic peroxides. Amongst them, only 1,2,4,5-tetraoxanes have two peroxide groups in the molecule and therefore may possess an enhanced pharmacological activity.[3] Unsymmetrical tetraoxanes hold better potential compared to symmetrical tetraoxanes due to wider structural scope.

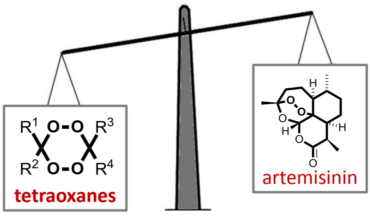

Challenges in the synthesis of tetraoxanes

Symmetrical tetraoxanes can be synthesized directly from carbonyl compounds, while unsymmetrical ones can only be prepared *via* a two-step procedure with *gem*-dihydroperoxides as intermediate products.[4]

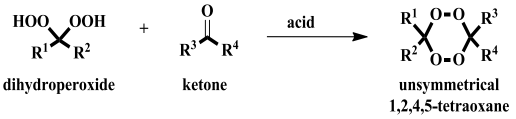

The main obstacle of acid catalysed peroxidations of ketones is selectivity due to formation of Baeyer-Villiger products and/or other cyclic products.[5] Most of all, it is of great importance to avoid formation of hexaoxonanes which have negligible bioactivity[6] and cannot be separated from desired product due to similar polarity.

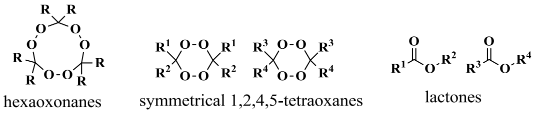

Optimization of reaction conditions

Cyclization of gem-dihydroperoxide and ketone gives unsymmetrical tetraoxane and, in many cases, also many side products, however, the selectivity depends on reaction conditions. Influence of solvent, time, temperature, addition of acid was studied and the best conditions are bolded.

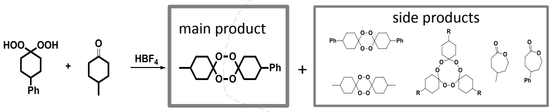

equiv. HBF4	solvent	T (min)	T (°C)	unsymm. TO (%)*	4PhTO (%)*	4MeTO (%)*	HO (%)*
1	TFE	5	RT	8	20	/	/
1	TFE	60	RT	4	21	/	/
1	MeCN	5	RT	52	/	/	/
1	MeCN	60	RT	10	9	/	/
1	TFE	5	0	62	/	/	16
1	TFE	60	0	33	4	/	/
1	MeCN	5	0	40	/	/	31
1	**MeCN**	**60**	**0**	**82**	**/**	**/**	**traces**
0,1	MeCN	5	RT	34	/	/	61
0,1	TFE	60	0	54	/	/	traces
2	TFE	5	0	41	/	/	traces

Applying method to other substrates

Optimized conditions were used for synthesis of several unsymmetrical tetraoxanes. However, the reactivity of *gem*-dihydroperoxide and ketone affects crucially reaction conditions for optimal conversion and selectivity and therefore for some reactions, additional optimization was needed.

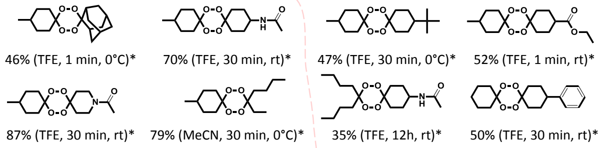

46% (TFE, 1 min, 0°C)*
70% (TFE, 30 min, rt)*
47% (TFE, 30 min, 0°C)*
52% (TFE, 1 min, rt)*
87% (TFE, 30 min, rt)*
79% (MeCN, 30 min, 0°C)*
35% (TFE, 12h, rt)*
50% (TFE, 30 min, rt)*

* Isolated yields and reaction conditions

Future perspectives for tetraoxanes

Tetraoxanes are potent antimalarial agents and the most promising candidate, RKA182, is undergoing preclinical trials.[7] Due to similiar structure and modes of action to artemisinins, which have exhibited broad spectra of bioactivities, tetraoxanes might have a bright future in the treatment of parasitic infections and also cancer.

antimalarial therapy?

antiparasitic therapy?

antitumor therapy?

References: [1]Jung M. t al., *Mini Rev Med Chem.* **2003**, *3,* 159-165. [2]Krishna S. *et al.*, *Trends Pharmacol Sci.* **2008,** *29*, 520-527. [3] Rawat DS. et al., *Med Res Rev.* **2012**, *32*, 581-610. [4]*Terent'ev AO. et al., Beilstein J Org Chem.* **2014**, *10*, 34-114. [5]Iskra J. et al.*, Bioorg Med Chem.* **2006,** *14*, 7790-7795; *Tetrahedron.* **2006**, *62*, 1479-1484; *JOC*. **2007**, *8*, 2491-2494. [6]Dong, Y. Et al; *Antimicrob. Agents Chemother.* **2007**, *51*, 3033-3035. [7]Flannery et al., Nature Rev Microbiol. **2013**, *11*, 849–862.

IPSSC: Oligomerization properties of G-quadruplex structures with GC end groups

Blaž Tašič[a,b], **Irena Drevenšek Olenik**[b,c], **Katarína Tlučková**[d], **Viktor Víglaský**[d], **Lea Spindler**[e,b]

a Study programme Nanosciences and Nanotechnologies, Jozef Stefan International Postgraduate School, Jamova 39, 1000 Ljubljana, Slovenia

b Department of Complex Matter, Jozef Stefan Institute, Jamova 39, 1000 Ljubljana, Slovenia

c Faculty of Mathematics and Physics, University of Ljubljana, Jadranska 19, 1000 Ljubljana, Slovenia

d Department of Biochemistry, Institute of Chemistry, Faculty of Sciences, P. J. Safarik University, Moyzesova 11, Kosice, Slovakia

e Faculty of Mechanical Engineering, University of Maribor, Smetanova 17, 2000 Maribor, Slovenia

blaz.tasic@gmail.com

Guanine-rich DNA sequences have the ability to grow into long nanowires made up of guanine (G:G:G:G) tetrads. These so called G-wires can be deposited on solid substrates and are due to their mechanical and thermal stability interesting candidates for molecular electronic devices. Our recent investigation showed that the sequence 5'-GCGGTG_4TGGCG-3' forms G-wires via formation of (G:C:G:C) tetrads [1]. To obtain more insight into the related self-assembly mechanism, we performed a comparative study of assembly properties of four analogous oligonucleotides: the above denoted one and the three similar ones with either 5', 3' or both GC-ends missing. Circular dichroism (CD) and polyacrylamide gel electrophoresis (PAGE) were used to investigate the structure, thermal stability, ageing, and the effect of adding different cations to the formation of G-quadruplex structures and to their oligomerization properties.

MEDNARODNA
PODIPLOMSKA ŠOLA
JOŽEFA STEFANA

JOŽEF STEFAN
INTERNATIONAL
POSTGRADUATE SCHOOL

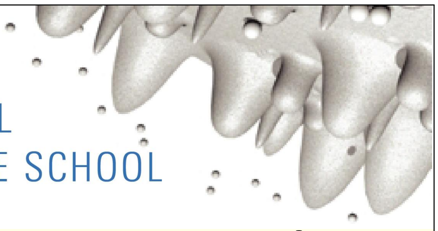

Oligomerization of DNA-quadruplex structures with GC end groups

Blaž Tašič[a,b], Irena Drevenšek Olenik[b,c,†], Katarína Tlučková[d], Viktor Víglaský[d], Mateus Webba Da Silva[e], Lea Spindler[f,b,‡]

†Supervisor, ‡Co-supervisor

[a] Study programme Nanosciences and Nanotechnologies, Jozef Stefan International Postgraduate School, Jamova 39, 1000 Ljubljana, Slovenia
[b] Department of Complex Matter, Jozef Stefan Institute, Jamova 39, 1000 Ljubljana, Slovenia
[c] Faculty of Mathematics and Physics, University of Ljubljana, Jadranska 19, 1000 Ljubljana
[d] Department of Biochemistry, Institute of Chemistry, Faculty of Sciences, P. J. Safarik University, Moyzesova 11, Kosice, Slovakia
[e] Faculty of Life and Health Sciences, University of Ulster, United Kingdom
[f] Faculty of Mechanical Engineering, University of Maribor, Smetanova 17, 2000 Maribor, Slovenia

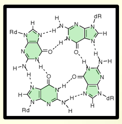

- Introduction -

Guanine-rich DNA sequences have the ability to grow into long nanowires made up of guanine (G:G:G:G) tetrads. These so called G-wires can be deposited on solid substrates and are due to their mechanical and thermal stability interesting candidates for molecular electronic devices. Previous investigations show that the sequence 5'-GCGGTG$_4$TGGCG-3' forms G-wires via formation of (G:C:G:C) tetrads [1]. To obtain more insight into the self-assembly mechanism, we investigated four analogous oligonucleotides: the above denoted one and three similar ones with either 5', 3' or both GC-ends missing. Circular dichroism (CD) and polyacrylamide gel electrophoresis (PAGE) were used to investigate the structure, thermal stability, effect of ageing, and the effect of adding different cations to our folded G-quadruplex structures.

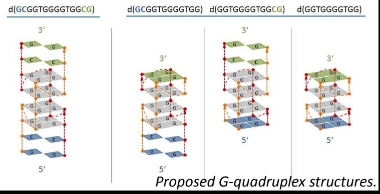

Proposed G-quadruplex structures.

- RESULTS -

Thermal stability

Formation of **basic G-quadruplex structures:**

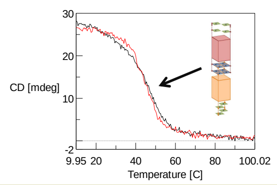

GCGGTG$_4$TGG**CG**
T_{m1} = 45 °C

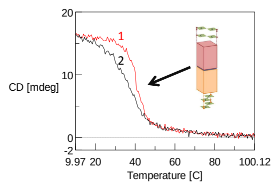

GGTG$_4$TGG**CG**
T_{m1} = 41 °C

Formation of **multimer G-quadruplex structures:**

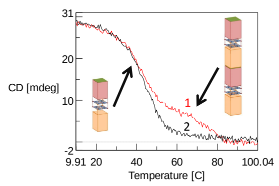

GCGGTG$_4$TGG
T_{m1} = 43 °C
T_{m2} = 72 °C

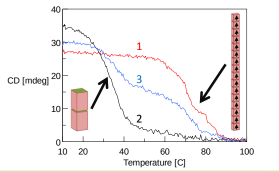

G$_2$TG$_4$TG$_2$
T_{m1} = 34 °C
T_{m2} = 73 °C

The thermal stability of basic quadruplex structures (T_{m1}) decreases in the order **GC**GGTG$_4$TGG**CG** > **GC**GGTG$_4$TGG > GGTG$_4$TGG**CG** > G$_2$TG$_4$TG$_2$. Results indicate that GC-ends significantly stabilise the basic quadruplex.

(1) Red - Heating, (2) Black – Cooling, (3) Blue - Heating after 3 days

Oligomerisation

GCG$_2$TG$_4$TG$_2$**CG** (lane 1) forms two structures which can be most probably attributed to a single quadruplex and to two quadruplexes linked by (G:C:G:C) tetrads. **GC**G$_2$TG$_4$TG$_2$ (lane 2) is characterised by a large smeared band which could result from two different structures in exchange and one hardly seen band higher above which represents 4 stacked quadruplexes. We observed only one strong band of G$_2$TG$_4$TG$_2$**CG** (lane 3) which we attribute to two stacked quadruplexes. G$_2$TG$_4$TG$_2$ (lane 4) shows a ladder effect which is typical for a long structure. We therefore conclude that this sequence forms long G-wires.

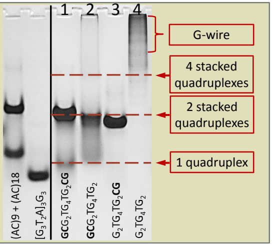

Ageing

Sequence G$_2$TG$_4$TG$_2$ (c = 1 mM) was heated to T= 95°C and left to slowly cool down. After denaturation progressive formation of larger structures is evident during the following days.

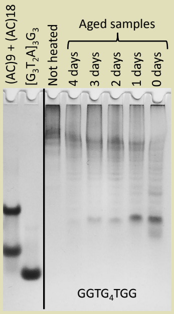

Concentration

If sequence G$_2$TG$_4$TG$_2$ is denaturated at a lower concentration (c = 0.06 mM) the stacking of quadruplexes is much slower.

Sequence GGTG$_4$TGG**CG** forms longer structures only in high concentration but these structures are not stable for a long time.

The other two sequences (**GC**GGTG$_4$TGG**CG** and **GC**GGTG$_4$TGG) formed after three days the same structures, regardless of their concentration.

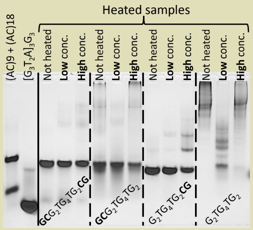

**All samples are 3 days old.*
Low concentration: C = 0.06 mM
High concentration: C = 1 mM

Effect of adding cations

We added different cations at high concentration to our samples and observed that ions thermally stabilized our G-quadruplexes in the following order **K$^+$ > Na$^+$ > Li$^+$** which agrees with the well established quadruplex-stabilising cation series.

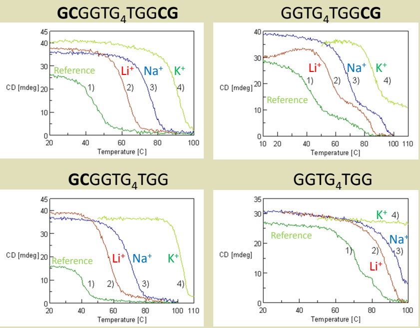

1) **100 mM NaCl**
2) **1 M LiCl** + 100 mM NaCl
3) **1 M NaCl**
4) **0,5 M KCl** + 100 mM NaCl

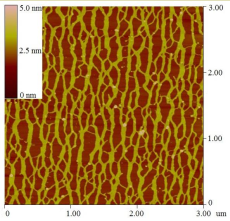

The sequence 5'-GCGGTG$_4$TGGCG-3' shows a promising ability to form extended networks of G-wires on mica substrates as documented by AFM [2].

- Conclusions -

- → CD melting curves and PAGE confirmed multimer structures in sequences **GC**G$_2$TG$_4$TG$_2$ and G$_2$TG$_4$TG$_2$.
- → Oligonucleotides with GC-ends are more thermally stable than those without GC-ends.
- → The addition of monovalent cations notably increased the thermal stability of the quadruplex structures.

- References -

[1] T. Ilc, P. Šket, J. Plavec, M. Webba da Silva, I. Drevenšek-Olenik, L. Spindler, "Formation of G-wires: The Role of G:C-base Pairing and G-quartet Stacking", *J. Phys. Chem. C*, 2013, 117 (44), pp 23208–23215.
[2] T. Troha, "Površinsko urejanje z gvaninom bogatih sekvenc DNK", diploma work, 2013.

The optimization of cleaning pre-treatment of aluminium alloy AA 7075

Urša Tiringer[1,2]
[1] Department of Physical and Organic Chemistry, Jožef Stefan Institute, Ljubljana, Slovenia [2] Jožef Stefan International Postgraduate School, Ljubljana, Slovenia
ursa.tiringer@ijs.si

Ingrid Milošev[1]
[1] Department of Physical and Organic Chemistry, Jožef Stefan Institute,
Ljubljana, Slovenia
ingrid.milosev@ijs.si

Aluminum and its alloys belong to light metals and are most commonly used in transportation industry. Present work aims to study the effect of cleaning of aluminium alloy of series AA 7075 with two different alkaline cleaners, first based on 0.01 M NaOH and exposed to 50% HNO_3 and second supplied by SurTec which is based on phosphates. According to the results obtained by electrochemical method, the cleaner based on NaOH and HNO_3 causes the passivation of AA 7075, while the potentiodynamic curve of surface cleaned with SurTec is similar to pure aluminium. XPS results show that both discussed cleaners remove contamination quite effectively. High resolution spectrum of Al 2p shows that in all samples aluminium is mostly present in its oxide state. Moreover, after both cleaning, with NaOH/HNO_3 and SurTec, the surface of AA 7075 becames almost superhydrophilic, while the untreated sample is hydrophilic.

MEDNARODNA
PODIPLOMSKA ŠOLA
JOŽEFA STEFANA

JOŽEF STEFAN
INTERNATIONAL
POSTGRADUATE SCHOOL

The optimization of cleaning pre-treatment of aluminum alloy AA7075

Urša Tiringer [a], Janez Kovač [b], Ingrid Milošev [a]
[a] Jožef Stefan Institute, Department of Physical and Organic Chemistry, Ljubljana, Slovenia
[b] Jožef Stefan Institute, Department of Surface Engineering and Optoelectronics, Ljubljana, Slovenia

Introduction

Aluminum and its alloys belong to light metals and are most commonly used in transportation industry. Despite the fact that pure aluminum resists corrosion well, its alloys may not be corrosion resistant in various environments. Many methods, such as chromate conversion coatings, anodization, sol-gel coatings, have been effective as aluminum protection against corrosion. Before any kind of treatment, it is necessary to perform a proper cleaning of the surface which will be treated. Most cleaning agents consist of acidic or alkaline media and can have a role of pickling agents, detergents, degreasing agents or of corrosion inhibitors. Present work aims to study the effect of cleaning of aluminum alloy AA7075 with alkaline cleaners. Two types of alkaline cleaners, first based on 0.01 M NaOH and 50% HNO_3, and second supplied by SurTec and is based on phosphates, were used [1 , 2, 3, 4].

Results

Figure 1: Polarization curves of AA 7075 samples cleaned with NaOH/HNO_3, SurTec phosphate cleaner and of untreated AA 7075 sample. Curves were recorded in 0.1 M NaCl.

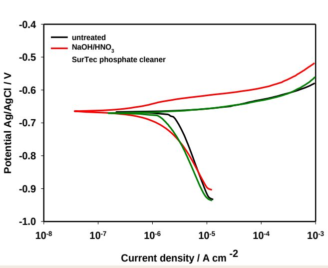

Figure 2: Top view of profiles obtained by profilometer and values of surface roughness (S_a) of utreated sample, sample cleaned with NaOH and HNO_3 and with SurTec phosphate cleaner. The colouring is according to the scale on the right which spans in the ± 1.5 µm. Image spot size 1 mm x 1mm range.

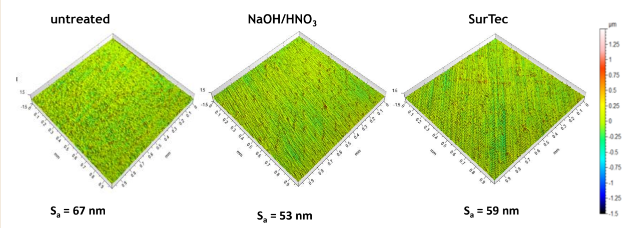

S_a = 67 nm

S_a = 53 nm

S_a = 59 nm

Figure 3: SEM analysis of sample AA 7075 cleaned with SurTec.

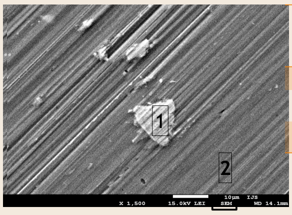

Table 1: EDXS analysis carried out at different locations at the treated sample of AA 7075 as denoted in in Fig. 3.

[at. %]	Al	Zn	Mg	O	Fe	Cu
Spectrum						
1	82.4	3.3	2.3	5.3	1.9	4.8
2	94.6	2.5	2.9	/	/	/

Figure 4: Images of water drops on the surface and the values of contact angles.

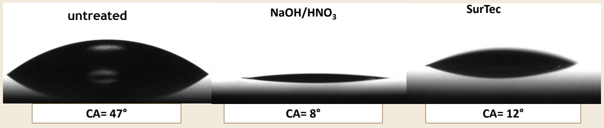

CA= 47°

CA= 8°

CA= 12°

Conclusions

- According to the results obtained by electrochemical method the cleaner based on NaOH and HNO_3 causes the passivation of AA 7075, while the potentiodynamic curve of surface cleaned with SurTec is similar to the curve of pure aluminum.

- Images and surface roughness obtained by profilometer do not indicate the difference in surfaces topography of differently treated samples.

- SEM image shows that the surface of AA 7075 cleaned with SurTec in addition to aluminum consists of alloying elements zinc, magnesium, iron and copper, while inclusion (1) is probably zinc oxide.

- After cleaning with NaOH/HNO_3 and with SurTec cleaner the surface of aluminum alloy AA 7075 becames almost superhydrophilic (CA≤10°), while the untreated is hydrophilic (CA = 47 °).

- High resolution spectrum of Al 2p shows that in all samples aluminum is mostly present in its oxide state. Energy of 74.2 eV denotes to the oxide state of aluminum and of energy 71.7 eV, elemental aluminum.

- Results obtained by XPS technique show that carbon contamination is reduced by cleaning. At the same time oxygen and aluminum content increased and alloying elements Mg and Si are removed. After using NaOH and HNO_3 the content of copper increased. After using SurTec cleaner the content of phosphorus increased.

Material and methods

Samples of aluminum alloys AA 7075 were ground using 2400 and 4000-grid SiC emery papers, ultrasonically cleaned in ethanol for 5 minutes, rinsed with deionized water and dried with a stream of N_2.
The nominal composition of AA 7075 in atomic percent is the folowing: 1.6 Cu, 2.5 Mg, 0.23 Cr and 5.6 Zn.
Samples of AA 7075 were divided into three groups:

- Followed by the first was immersed in the 0.01 M NaOH for 3 minutes and than in 50 % HNO_3 for 30 seconds.
- The second was cleaned using SurTec product, which was formed by combination of 3 % SurTec132 liquid recyclable builder and of 0.5 % SurTec089 recyclable detergent component. The sample was immersed in the mixture for three minutes at 40°C.
- The third was untreated sample.

The comparison of cleaners was carried out by electhrochemical polarization method, X-ray photoelectron spectroscopy, profilometer, tenziometer and scanning electron microscopy.

Electrochemical measurement were performed in 0.1 M NaCl at room temperature. An Autolab corrosion cell with a volume 0.350 L was used. The working electrode was embedded in a Teflon holder. Graphite electrode served as a counter electrode and saturated calomel electrode (SCE) was a reference electrode.
After 1 h stabilization at open circuit potential (OCP) measurements were performed in the following order: linear polarization, ±10mV versus OCP, using a scan rate of 0.1mV/s and potentiodynamic measurements starting from -250 mV vs. OCP up to -0.5 V using a scan rate of 1 mV/s.

The X-ray photoelectron spectroscopy (XPS) analysis was carried out on the PHI-TFA XPS spectrometer (Physical Electronics Inc.). The vacuum during the XPS analyses was in the range of 10^{-9} mbar. The analyzed area was 0.4 mm in diameter and the analyzed depth was about 3 - 5 nm. Sample surfaces were excited by X-ray radiation from monochromatic Al source at photon energy of 1486.6 eV. Spectra were analyzed by a Multipak software, version 8.0 (Physical Electronics Inc company) [5].

Surface roughness (S_a) was measured with the profilometer ZEISS Axio CSM 700.
Scanning electron microscopy (SEM) images were taken with JEOL JSM-7600F microscope equiped with chemical analyis (EDXS).
Contact angles (*CA*) were measured with tensiometer Krüss DSA 20E.

Figure 5: The concentration of elements obtained by XPS after various surface treatments: untreated, exposed to 0,01 M NaOH and HNO_3 and exposed to SurTec cleaner.

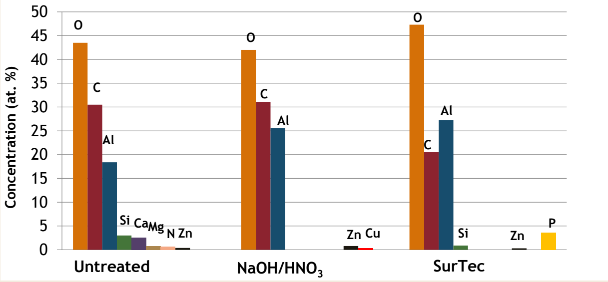

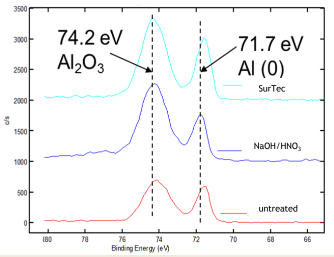

Figure 6: High resolution spectra of Al 2p obtained by XPS technique show the formation of aluminum oxide on differently cleaned samples.

References

1. Vargel C. Corrosion of aluminium. 1st ed. Amsterdam, The Netherlands: ELSEVIER; 2004

2. Davis J. R. Corrosion of aluminum and aluminum alloys. 1st ed. United States of America: ASM International; 1999: 10-23.

3. Grilli R. Conversion coatings for aluminium alloys: a surface investigation for corrosion mechanisms. Doctor Degree. University of Surrey: UK: 2010.

4. Joshi S., Fahrenhiltz W.G., O`Keefe M.J. *Effect of alkaline cleaning and activation on aluminum alloy 7075-T6.* Applied surface science. 2011, **257**: 1859-1863.

5. Kufman G. Introduction to aluminum alloys and tempers. 1st. ed. ASM International; 2000.

Kazalo Avtorjev (List of Authors)

Sodelujoča podjetja in organizacije:

Institut
”Jožef Stefan”
Ljubljana, Slovenija

ISO
Fd
Food
ERA Chair
Safety
Quality
Traceability

greener

ADORA

IZVOR
by OriginTrail

SPIRIT
SLOVENIJA
JAVNA AGENCIJA
I FEEL SLOVENIA

REPUBLIKA SLOVENIJA
MINISTRSTVO ZA GOSPODARSKI
RAZVOJ IN TEHNOLOGIJO

LJUBLJANSKI UNIVERZITETNI
INKUBATOR


ECO
samples
compounds
tea
bread
products
high
mercury
temperature
activity
separation
PPCPs
provide
release
environment
care
milk
gas
MoS2
fate
results
fractionation
chromatographic
organic
exist
applied
confirm
spite
run
work
stable
materials
different
enables
Monolithic
information
human
data
ketoprofen
catalytic
columns
monolithic
structure
chromatography
coal
50Cr
years
low
effects
presence
experiments
isotope
analysis


new
materials
magnetic
nanoparticles
IPS
high
applications
methods
network
work
data
using
properties
process
system
human
sensor
coding
sensors
compounds
activity
model
drug
based
samples
learning
wireless
body
devices

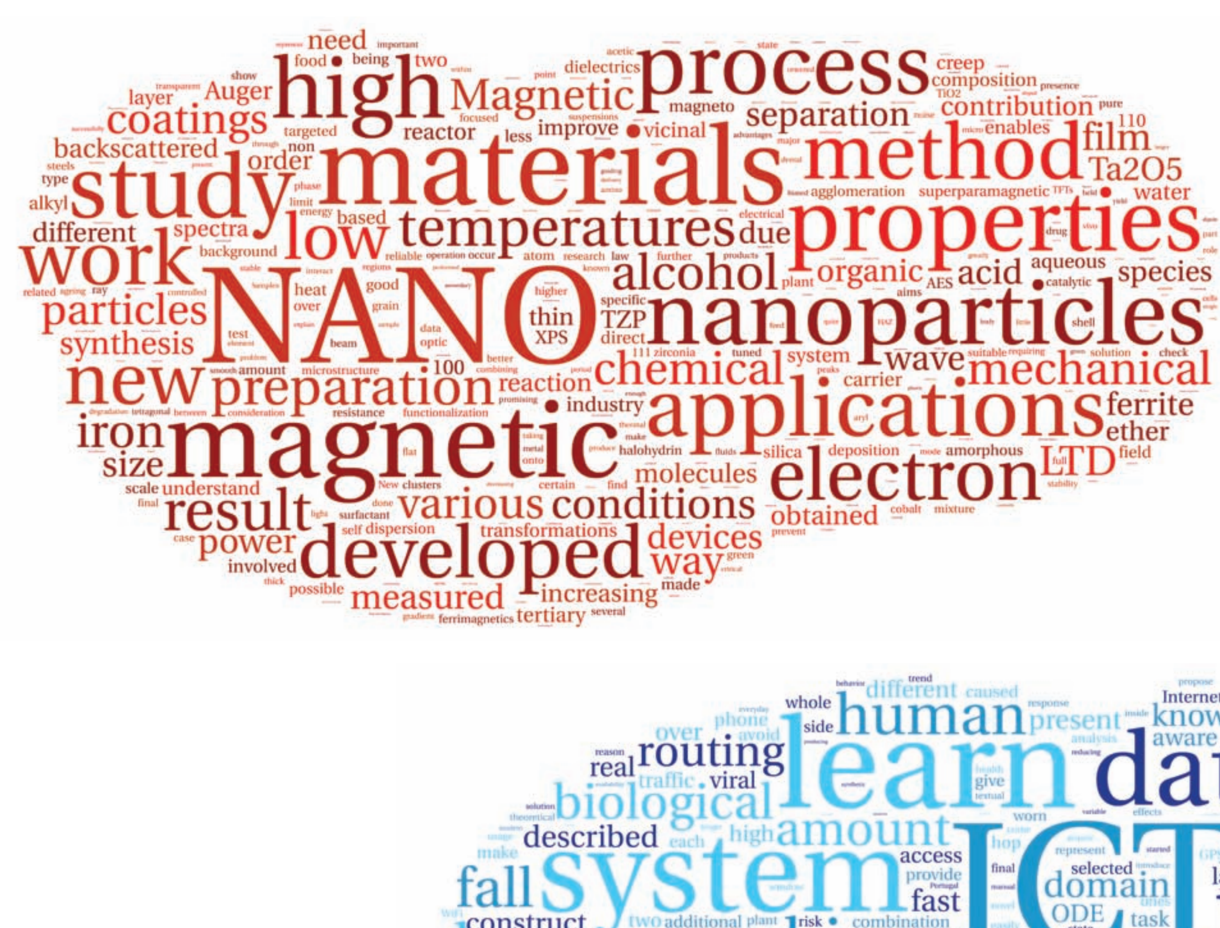
NANO
materials
magnetic
nanoparticles
applications
properties
process
high
method
study
work
low
new
developed
electron
result
temperatures
alcohol
chemical
mechanical
preparation
particles
synthesis
coatings
Magnetic
various
conditions
iron
power
measured
film
Ta2O5
ferrite
LTD
species
wave
TZP
XPS
separation
Auger
reactor
improve
increasing
devices

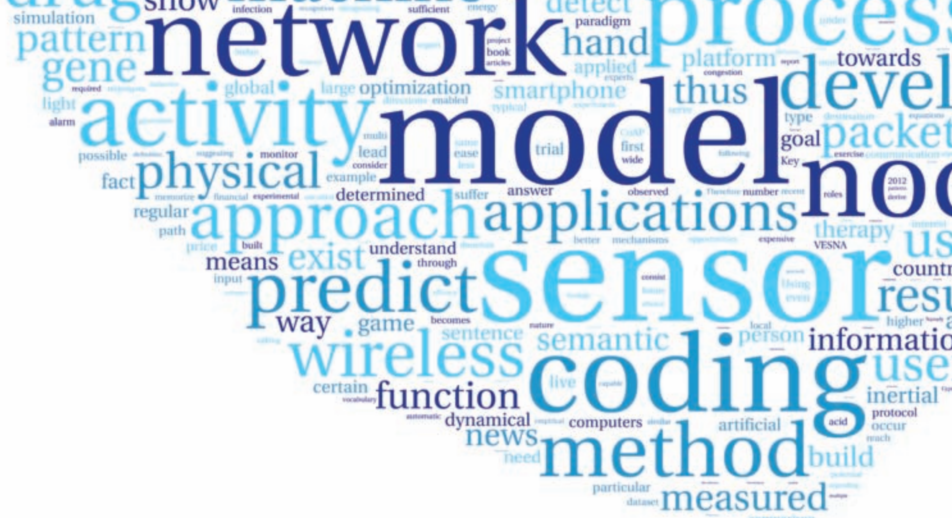
ICT
learn
data
system
rule
network
process
model
node
sensor
coding
method
activity
approach
applications
develop
predict
wireless
human
routing
biological
machine
new
drug
fall
amount
domain
packet
physical
user
using
result
semantic
information
function
measured
knowledge
pattern
gene
detect
show
build

**MEDNARODNA
PODIPLOMSKA ŠOLA
JOŽEFA STEFANA**

**JOŽEF STEFAN
INTERNATIONAL POSTGRADUATE SCHOOL**

Jamova 39, SI-1000 Ljubljana

**T +386 (0)1 477 31 00
F +386 (0)1 477 31 10**

**E info@mps.si
www.mps.si**

ISBN 9789619287194
9 789619 287194

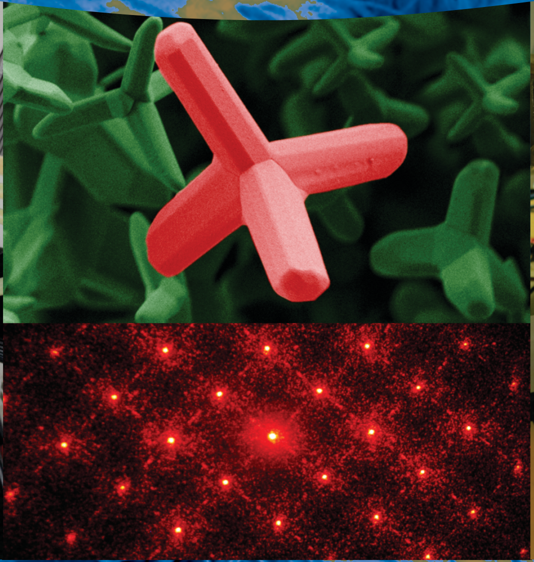

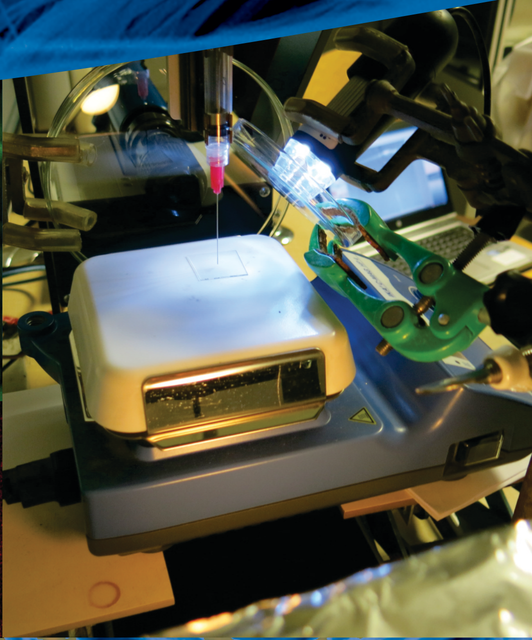

20. - 21. 05. 2015, Ljubljana